Environmental Science and Ecotechnology 18 (2024) 100313

Contents lists available at ScienceDirect

Environmental Science and Ecotechnology

journal homepage: www.journals.elsevier.com/environmental-science-and-ecotechnology/

Original Research

Sedimentary records of contaminant inputs in Frobisher Bay, Nunavut

Meaghan C. Bartley [a, b, *], Tommy Tremblay [c], Amila O. De Silva [d], C. Michelle Kamula [a, 1], Stephen Ciastek [a], Zou Zou A. Kuzyk [a, b, e, **]

[a] Centre for Earth Observation Science, Clayton H. Riddell Faculty of Environment, Earth and Resources, University of Manitoba, Winnipeg, Manitoba, R3T 2N2, Canada
[b] Department of Environment and Geography, Clayton H. Riddell Faculty of Environment, Earth and Resources, University of Manitoba, Winnipeg, Manitoba, R3T 2N2, Canada
[c] Canada-Nunavut Geoscience Office, Iqaluit, Nunavut, X0A 0H0, Canada
[d] Environment and Climate Change Canada, Burlington, Ontario, L7S 1A1, Canada
[e] Department of Earth Sciences, Clayton H. Riddell Faculty of Environment, Earth and Resources, University of Manitoba, Winnipeg, Manitoba, R3T 2N2, Canada

ARTICLE INFO

Article history:
Received 8 January 2023
Received in revised form
5 September 2023
Accepted 11 September 2023

Keywords:
Arctic sediments
Mercury
Polycyclic aromatic hydrocarbons (PAHs)
Polychlorinated biphenyls (PCBs)
Per and polyfluoroalkyl substances (PFASs)
Persistent organic pollutants (POPs)

ABSTRACT

Contaminants, such as polychlorinated biphenyls (PCBs), polycyclic aromatic hydrocarbons (PAHs), heavy metals, and per and polyfluoroalkyl substances (PFASs), primarily reach the Arctic through long-range atmospheric and oceanic transport. However, local sources within the Arctic also contribute to the levels observed in the environment, including legacy sources and new sources that arise from activities associated with increasing commercial and industrial development. The City of Iqaluit in Frobisher Bay, Nunavut (Canada), has seen rapid population growth and associated development during recent decades yet remains a site of interest for ocean protection, where Inuit continue to harvest country food. In the present study, seven dated marine sediment cores collected in Koojesse Inlet near Iqaluit, and from sites in inner and outer Frobisher Bay, respectively, were analyzed for total mercury (THg), major and trace elements, PAHs, PCBs, and PFASs. The sedimentary record in Koojesse Inlet shows a period of Aroclor 1260-like PCB input concurrent with military site presence in the 1950–60s, followed by decades of input of pyrogenic PAHs, averaging about ten times background levels. Near-surface sediments in Koojesse Inlet also show evidence of transient local-source inputs of THg and PFASs, and recycling or continued slow release of PCBs from legacy land-based sources. Differences in PFAS congener composition clearly distinguish the local sources from long-range transport. Outside Koojesse Inlet but still in inner Frobisher Bay, 9.2 km from Iqaluit, sediments showed evidence of both local source (PCB) and long-range transport. In outer Frobisher Bay, an up-core increase in THg and PFASs in sediments may be explained by ongoing inputs of these contaminants from long-range transport. The context for ocean protection and country food harvesting in this region of the Arctic clearly involves both local sources and long-range transport, with past human activities leaving a long legacy insofar as levels of persistent organic pollutants are concerned.

1. Introduction

Although contaminant levels in Arctic environments are often lower than those in temperate locations close to cities and industrial areas, contaminant studies in the Arctic remain important. Traditional harvesting provides a potential pathway for transferring contaminants directly from the environment, through the food web, to top consumers and humans, especially Inuit [1]. For some contaminants, pollution emissions around the globe are increasing in response to warming and increased wildfires [2]. Inside the

* Corresponding authors. CEOS, University of Manitoba, 125 Dysart Rd., Winnipeg, Manitoba, R3T 2N2, Canada.
** Corresponding author. CEOS, University of Manitoba, 125 Dysart Rd, Winnipeg, Manitoba, R3T 2N2, Canada.
E-mail addresses: bartleym@myumanitoba.ca (M.C. Bartley), tommy.tremblay@nrcan-rncan.gc.ca (T. Tremblay), amila.desilva@ec.gc.ca (A.O. De Silva), michelle.kamula@umanitoba.ca, michelle.kamula@dfo-mpo.gc.ca (C. Michelle Kamula), stephen.ciastek@umanitoba.ca (S. Ciastek), zouzou.kuzyk@umanitoba.ca (Z.Z.A. Kuzyk).
[1] Current address: Fisheries and Oceans Canada, Winnipeg, Manitoba, R3T 2N6, Canada.

https://doi.org/10.1016/j.ese.2023.100313

Arctic, altered hydrologic cycles [3] and biogeochemical processes [4] may alter the contaminant exposure for organisms at the base of the marine food web. Furthermore, Arctic populations and air traffic and the number of industrial developments, such as sea ports, have been growing, potentially increasing the relative importance of local contaminant sources, and this trend will likely continue with the longer ice-free season projected for the future [5].

Certain contaminants are particularly concerning in the Arctic due to their persistence, the large volumes released in commercial/industrial source areas, and their potential for bioaccumulation and biomagnification. These include polychlorinated biphenyls (PCBs), polycyclic aromatic hydrocarbons (PAHs), heavy metals (e.g., cadmium, lead, and mercury) [6], per and polyfluoroalkyl substances (PFASs) [7], and others. Generally, there are two main sources of contaminants in the Arctic: long-range transport (LRT) and local sources. LRT through global atmospheric and ocean currents carries anthropogenic contaminants to the Arctic [6]. Local sources include military sites established across the north in the 1950s that used contaminants, such as PCBs and pesticides [8–10], and, more recently, wastewater discharges from communities, which may contain "new contaminants", including pharmaceuticals and PFASs [11].

The predominant focus in numerous studies has been on LRT as the primary source of pollutants in most Arctic regions [6,9,12–16]. With clean ship-board measurements cf. [17] and passive sampler deployments cf. [18], large-scale contaminant transport pathways in the Arctic Ocean have become better understood. However, less is known about how local sources and LRT collectively contribute to total contaminant pools (and hence cumulative contaminant exposures) near northern population centres. Assessments of priority contaminants and their source contributions near northern communities are particularly important in areas where human activities have recently changed or increased [11,19–22]. Communities where traditional harvesting remains a priority alongside increasing industrial development are obvious priorities for research.

A major population centre in the Canadian Arctic that has seen increased human activity during recent decades is the City of Iqaluit in Frobisher Bay, Nunavut. There are several possible local sources of contaminants near the coastal environment of inner Frobisher Bay in addition to LRT. The City of Iqaluit's population has increased dramatically in the past 30 years [23], accompanied by major infrastructure development [22]. Possible active sources of contaminants near the City include a sewage lagoon, garbage dumps, small-craft harbours, and an airport. Previous studies found the sewage lagoon to be a source of disturbance to the receiving waters of Koojesse Inlet [20,21,24]. Major landfill fires have occurred on several occasions, the most recent in 2014 [25]. Additionally, the Iqaluit area hosted a military site [22], which was in operation from 1946 to 1963 [26] and abandoned in 1972 [8]. Government-led remediation in the late 1990s and the 2010s included demolition, excavation, implementation of an engineered landfill on-site, and removal and shipment of certain hazardous materials outside of Iqaluit [27]. Despite the cleanup efforts at this site, human activities sometimes inadvertently alter the release and transport of contaminants and thereby lead to enhanced contaminant fluxes into coastal environments. Environmental change associated with climate warming and sea-level rise also can alter contaminant release from previously secure locations cf. [28]. Lastly, in addition to potential land-based and airborne contaminant sources near Iqaluit, shipping activity near the community has increased dramatically during the past few decades [29] and is expected to increase further following the development of a new deep-water port over 2018–2022.

The coastal marine environment near Iqaluit, called Koojesse Inlet, has been investigated in recent years to assess wastewater impacts [11,20,21,24,30], food web dynamics of THg [31], and surface sediment distribution of PAHs [32]. However, the evolution of contaminant sources affecting Koojesse Inlet during the past decades and recent years, as can be obtained from dated sedimentary records, is lacking. Here, we use profiles of THg, PAHs, PCBs, and PFASs in seven dated sediment cores to assess past and present contaminant inputs to Frobisher Bay, Nunavut. We compare contaminant profiles, inventories, and compositions across sites in Koojesse Inlet, inner Frobisher Bay, and outer Frobisher Bay to assess the relative importance of local and distant contaminant sources. The results provide the first multi-contaminant baseline data set for the Iqaluit area, which we believe to be relevant for future planning and assessment purposes in the context of local desires to maintain an environment suitable for harvesting country foods.

2. Methods

2.1. Study area

Frobisher Bay, Nunavut (Fig. 1) is a 230 km long and 20–40 km wide inlet of the Labrador Sea, located along southeastern Baffin Island [33]. Outer Frobisher Bay is 200 km long and generally less than 300 m deep (Fig. 1a). Inner Frobisher Bay is separated from outer Frobisher Bay by a chain of islands about 35 nautical miles southeast of the City of Iqaluit [34]. Inner Frobisher Bay is an embayment 70 km long, usually less than 100 m deep, with a tidal range of about 11 m [22,35]. Koojesse Inlet, a shallow embayment located within inner Frobisher Bay (Fig. 1b), is 4 km long [22] and is characterized by extensive tidal flats [24,35].

2.2. Sampling and data collection

The collection, processing, and preliminary analytical and sedimentological interpretations of the sediment cores used in this study were described previously [22]. Sediment samples were collected from 20 sites in Koojesse Inlet, Frobisher Bay, in 2017. This sampling occurred in 2017 before the dredging activities for the port construction started [22]. In 2018, two additional cores were collected, one along the central axis of inner Frobisher Bay (core Bell_10) and one in outer Frobisher Bay (core 12C). These latter locations are well removed from the site of port construction. Seven sediment cores from 2017 to 2018 were selected for contaminant analysis and will be discussed here (Fig. 1, Table 1). The cores from Koojesse Inlet were collected from Research Vessel (RV) *Nuliajuk* in 2017 using an Ocean Instruments 25 × 25 × 50 cm GMX-25 GOMEX box corer. In 2018, cores Bell_10 and 12C were collected from CCGS *Amundsen* using an Ocean Instruments 50 × 50 × 50 cm BX-650 MK-III box corer. Sediment cores were sub-sectioned in 1 or 2-cm intervals throughout the length of each core. Sediment processing is described in the Supplementary Information (SI). Analyses were performed on one core from each of the sampling sites.

2.3. Laboratory analysis

Chemical analysis was completed by individual labs with specific expertise. There is inherent variability in the quality assurance/quality control (QA/QC) approach implemented by each analytical laboratory. However, all labs evaluated precision through replicates, accuracy through standard reference materials, and background contamination through blanks. Most of the analyses were conducted in accordance with long-established standardized methods and/or are based on previously published methods, as

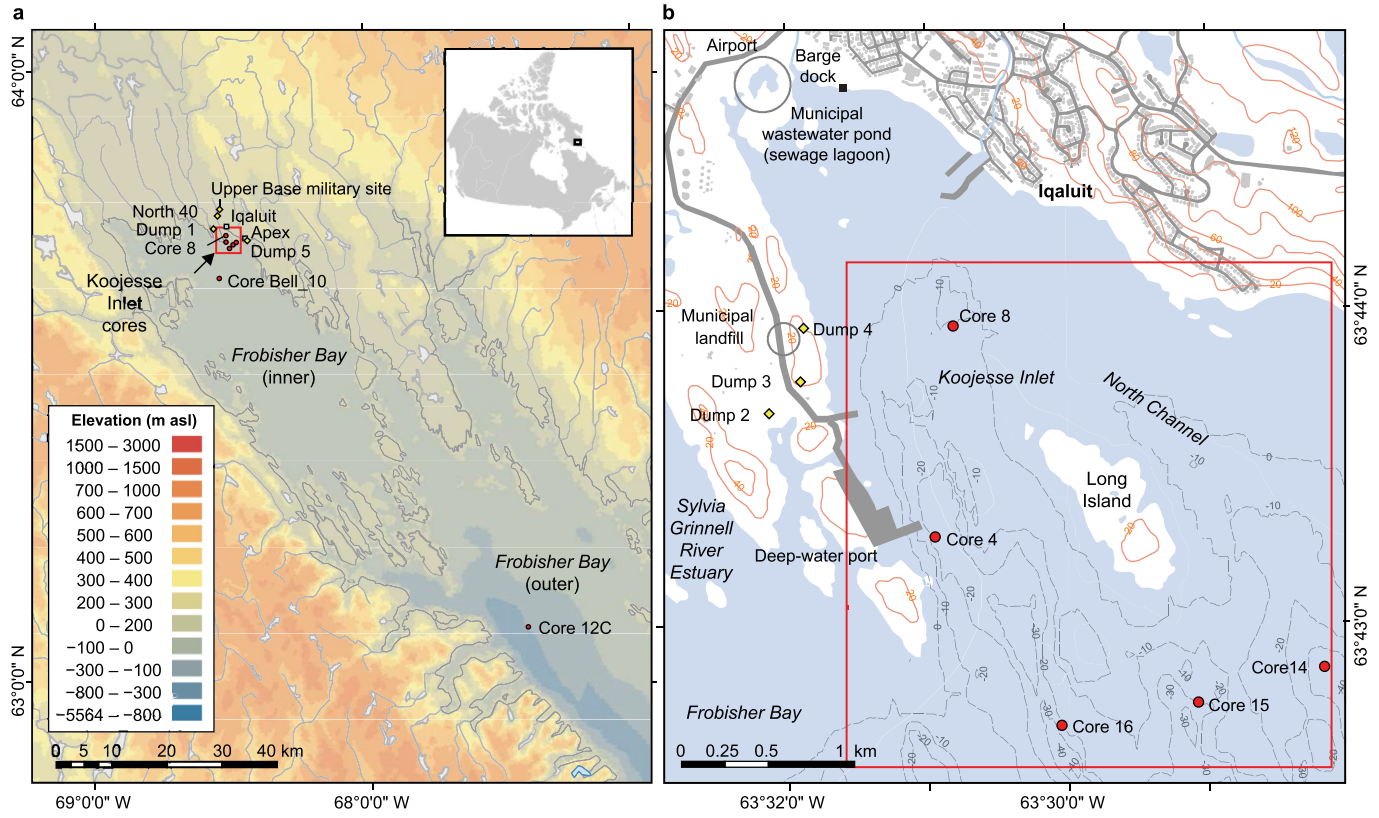

Fig. 1. **a**, Map of the sampling sites in inner and outer Frobisher Bay where sediment cores were collected in 2017 and 2018. **b**, Map of the sampling sites in Koojesse Inlet near the City of Iqaluit that overlaps the same region of inner Frobisher Bay. Red circles indicate the seven sites where sediment cores were collected. Yellow diamonds in panel **b** indicate abandoned solid waste disposal sites. The red box in panel **b** indicates the area within Koojesse Inlet where sediment cores were collected.

Table 1
Core ID, date of collection, geographic coordinates, water depth, total length of core recovered, and distance from Iqaluit's sewage lagoon to the sites for the sediment cores collected from Frobisher Bay, Nunavut.

Core ID	Date	Longitude	Latitude	Water depth (m)	Core length (cm)	Distance from Iqaluit's sewage lagoon (km)
Koojesse Inlet						
4	2017-10-06	−68.5158	63.7213	10	20	2.8
8	2017-10-06	−68.5135	63.7324	6	29	1.8
14	2017-10-07	−68.4696	63.7143	21	14	4.8
15	2017-10-07	−68.4846	63.7123	24	19	4.5
16	2017-10-07	−68.5009	63.7113	15	19	4.2
Other Frobisher Bay Sites						
Bell_10	2018-07-25	−68.5389	63.6614	89.6	20	9.2
12C	2018-07-25	−67.43	63.0813	389	12	92

noted in the text. Further details from each laboratory and QA/QC are presented in the SI. Only select slices within each core were selected for contaminant analysis. Therefore, data gaps in the figures represent sediment slices that were not analyzed for that particular class of contaminants.

Downcore activities of ^{210}Pb (lead), ^{226}Ra (radium), and ^{137}Cs (cesium) were indirectly measured in cores 4, 8, and 16 by the alpha-counting method at Flett Research Ltd. In Winnipeg, MB, following a method modified from Ref. [36]. Gamma emissions of ^{210}Pb, ^{226}Ra, and ^{137}Cs were measured in cores 14, 15, Bell_10, and 12C at the Environmental Radiochemistry Laboratory (ERL) at the University of Manitoba, Winnipeg, MB. Cores 4, 8, and 16 were also analyzed for ^{137}Cs at ERL. Further details on radioisotope analysis are provided in the SI. Excess ^{210}Pb was calculated by subtracting supported ^{210}Pb from the total ^{210}Pb. Supported ^{210}Pb was estimated from either the ^{226}Ra activity in the same section or the total ^{210}Pb in the bottom section of the core. Sediment accumulation rates (SAR) were calculated by fitting the natural log of excess ^{210}Pb profiles to outputs of a one-dimensional two-layer advection-diffusion model. The model assumes a surface mixed layer with a significant mixing rate underlain by a layer with minimal mixing (see Ref. [37] for details). Mass accumulation rates (MAR) were calculated from the SAR. Inventories of excess ^{210}Pb and ^{137}Cs were calculated by summing the mass-depth activities down-core until the activity was no longer detected.

At the University of British Columbia, total carbon and nitrogen (TC and TN), total inorganic carbon (TIC), total organic carbon (TOC), stable carbon (δ^{13}C), and nitrogen (δ^{15}N) isotope compositions were measured.

Sediment subsamples were analyzed for major and trace elements (see Table S1 for elements quantified) at Institut national de la recherche scientifique (INRS) laboratories, Quebec City, QC,

following US EPA Method 200.7 and US EPA Method 200.8. THg was measured at the Centre for Earth Observation Science (CEOS) laboratory in Winnipeg, MB, according to US EPA Method 7473.

Sediment samples were analyzed for 15 PAHs (see list in Table S2) at the Petroleum Environmental Research Laboratory at CEOS in Winnipeg, MB, following US EPA Method 3630C. Samples were analyzed for 162 individual or co-eluting PCB congeners (see list in Table S3) at the ALS Global Labs in Burlington, ON, according to US EPA Method 1668C. Samples were analyzed for 26 PFASs (see target list in Table S4) at the Environment and Climate Change Canada lab in Burlington, ON, using previously reported methods [14] based on the addition of stable isotopes, solvent extraction with carbon clean-up and analysis by liquid chromatography tandem mass spectrometry.

2.4. Statistical analysis

Prior to statistical analysis, PAH and PCB concentrations were blank-corrected due to the detection of trace amounts in the blanks. PFAS concentrations were blank-subtracted and recovery corrected by the Environment and Climate Change Canada laboratory. Zero was used to replace the "non-detect" values for contaminants with concentrations below the limit of detection (LOD). Salt correction factors for each core slice were calculated from the percent moisture for each sample and salinity. Salinity was assumed to be 31.12 psu for cores 4, 8, 14, 15, 16, and Bell_10, based on data collected from a Koojesse Inlet station in 2018 at a depth of 6 m (C. Lewis, Fisheries and Oceans Canada, pers. Comm., July 2022). Salinity was assumed to be 32.5 psu for core 12C. ^{137}Cs, ^{210}Pb, TC, OC, δ^{13}C, TN, δ^{15}N, major and trace element, THg, PAH, PCB, and PFAS data were multiplied by the salt correction factors to account for the amount of salt in each sample. Porosity values were corrected for salt using percent moisture, salinity, water density, and solids density (assumed to be 2.65 g cm^{-3}). All data are reported in dry weight (dw). Data analysis, statistics, and figures were conducted in RStudio version 4.2.3 [38]. The 13–14 cm slice in core 4 was omitted from THg analysis due to its unusually high concentration.

Fifteen PAHs were summed to provide a total concentration ($\sum$PAHs; Table S2). Diagnostic ratios of fluoranthene divided by the sum of fluoranthene and pyrene (Fla/[Fla + Pyr]) and benz(a) anthracene divided by the sum of benz(a)anthracene and chrysene (BaA/[BaA + Chr]) were calculated to assess pyrogenic vs. petrogenic PAH sources. The 10–12 cm slice in core Bell_10 was omitted from PAH analysis due to potential contamination during shipboard sample collection.

PCB-011, a commonly found but unintentionally produced PCB congener [39], was removed from the analysis due to its high concentration in most samples. One hundred and sixty-one congeners were summed to provide a total concentration ($\sum$PCBs; Table S3, excluding PCB-011). PCB data was normalized by calculating the percent contribution to the total for the 92 congeners detected regularly in the samples ($\geq$50% of all samples) to conduct Principal Component Analysis (PCA). Two samples were removed from the PCA due to being outliers in the factor scores (the 18–20 cm slice in core Bell_10 and the 10–12 cm slice in core 12C). Factor scores for principal components 1 (PC1) and 2 (PC2) were subjected to One-way Analysis of Variance (ANOVA), and if the results were statistically significant, Tukey Honest Significant Differences (Tukey HSD) tests. The composition of the industrial PCB mixture Aroclor 1260, retrieved from Ref. [40], was converted to the percent contribution of the same 92 congeners and projected onto the factor scores plot.

The analytical list of PFAS targets consisted of C4 to C16 perfluorocarboxylic acids (PFBA, PFPeA, PFHxA, PFHpA, PFOA, PFNA, PFDA, PFUnDA, PFDoDA, PFTriDA, PFTeDA, PFHxDA), perfluorosulfonic acids (PFBS, PFHxS, PFOS, PFECHS, PFDS), novel ether and/or chlorine substituted PFAS (HFPO, ADONA, 8Cl-PFOS, 9Cl-PFONS, 11-PFONS), fluorotelomer carboxylic acids (5:3 FTCA, 7:3 FTCA, 8:3 FTCA), and perfluorooctane sulfonamide (FOSA; Table S4). Among these, nine analytes had a detection frequency of >70% in the samples: C7 to 13 perfluorocarboxylic acids, PFOS, and FOSA. The novel PFASs, PFPeA, PFHxDA and PFBS had detection frequencies <10% and were excluded from data interpretation. The following 18 PFASs had detection frequencies >10% and were summed to provide a total concentration ($\sum$PFASs): PFBA, PFHxA, PFHpA, PFOA, PFNA, PFDA, PFUnDA, PFDoDA, PFTriDA, PFTeDA, PFHxS, PFOS, PFECHS, PFDS, FOSA, 5:3 FTCA, 7:3 FTCA, and 8:3 FTCA.

3. Results

3.1. Sediment properties and sedimentation rates

Sedimentation rates and associated parameters interpreted from radioisotope profiles in the sediment cores were reported previously [22] and are summarized in Table 2. The sedimentation rates were estimated by fitting a two-layer advection diffusive model that incorporates a surface mixed layer to the profiles of excess ^{210}Pb in the cores and verified against ^{137}Cs. In core Bell_10, the ^{137}Cs activity was low and detectable only in the upper couple of sections; the estimated sedimentation rate of 0.19 cm yr^{-1} should be viewed as a maximum value. For core 12C, the ^{210}Pb-derived sedimentation rate of 0.15 cm yr^{-1} was verified by the core's ^{137}Cs profile. This sedimentation rate agrees well with previously published sedimentation rates for Canadian Arctic shelf sediments at similar water depths [41]. The intrinsic time resolution within core 12C was about 33 years.

Core 8 and other Koojesse Inlet sediments generally had thicker surface mixed layers (10 cm) and faster surface mixing rates (10–20 cm^2 yr^{-1}) compared to cores Bell_10 and 12C (Table 2), probably due to increased bioturbation and mixing from tidally generated currents. These sites were near the shore, within less than 5 km of the Iqaluit sewage lagoon (a feature easily identified in satellite imagery), and in water depths less than 25 m (Table 2). Although Koojesse Inlet is relatively protected insofar as northerly and westerly fetch, and potential waves are concerned, it does have a large tidal range (12.4 m [35]) and a benthic community that may cause bioturbation [42]. Core 8 contained a large inventory of ^{137}Cs (Table 2; Fig. S1), including a pronounced ^{137}Cs peak between 25 and 30 cm depth. Considering both ^{210}Pb and ^{137}Cs profiles, we estimate a sedimentation rate in this core of 0.5 cm yr^{-1} and an intrinsic time resolution of about 20 years (Table 2). The distribution of ^{137}Cs in the core compared well with the simulated profile for ^{137}Cs deposited over a decade starting in 1954, as predicted by a numerical advective-diffusive model constrained using these parameters (Fig. S1). The ^{137}Cs input function used in the modelling derived from the record of atmospheric fallout from nuclear weapons testing [43], which has been used to reproduce ^{137}Cs penetration depths in Arctic shelf sediments previously cf [37,41,44]. The record of contaminant input in core 8 from Koojesse Inlet thus spans about 60 years, during which various forms of local and international development have occurred.

3.2. Organic matter content and composition

Average concentrations of organic carbon (OC) differed markedly among the cores (Fig. 2), with significantly higher OC concentrations in core 12C (2.18 ± 0.56%, n = 11) compared to cores 8 and Bell_10. The latter cores had average concentrations of 1.09 ± 0.34% (n = 15) and 1.28 ± 0.16% (n = 8), respectively (Fig. 2a).

Table 2
Sediment core properties, sedimentation rates, and parameters. SML = Surface mixed layer; Kb_1 = upper layer mixing rater; SAR = sedimentation velocity (95% confidence limit); MAR = mass accumulation rate (95% confidence limit); $\sum^{210}Pb_{ex}$ and $\sum^{137}Cs$ = sediment inventories (± standard deviation), and intrinsic time resolution.

Core ID	SML (cm)	Kb_1 ($cm^2\ y^{-1}$)	Φ_{avg}	SAR (cm y^{-1})	MAR (g $cm^{-2}\ y^{-1}$)	$\sum^{210}Pb_{ex}$ ± 1SD (dpm cm^{-2})	$\sum^{137}Cs$ ± 1SD (dpm cm^{-2})	Intrinsic time resolution (y)	Comments
Koojesse Inlet									
4	10	12	0.56	0.59 (0.35–1.82)	0.72 (0.40–2.10)	16.6 ± 0.6	0.5 ± 0.1	17	Low ^{137}Cs activity. Unable to validate.
8	10	20	0.68	0.5 (0.5–1.5)	0.5 (0.5–1.4)	29.9 ± 1.4	4.0 ± 0.2	20	SAR is not well constrained by ^{210}Pb but the onset of ^{137}Cs at 25–30 cm depth gives constraint.
14	-	-	-	-	-	31 ± 2	0.13	-	Highly mixed $^{210}Pb_{ex}$ profile not suitable for the model. ^{137}Cs activity low.
15	7	15	0.73	0.46 (0.18–0.91)	0.37 (0.15–0.73)	28.6 ± 1.4	-	15	^{137}Cs data not available.
16	8	7	0.65	0.2 (0.06–0.22)	0.2 (0.06–0.23)	14.2 ± 1.1	0.9 ± 0.2	28	^{210}Pb influenced by mixing, but ^{137}Cs onset at 14 cm provides constraint.
Other Frobisher Bay sites									
Bell_10	7	8	0.65	0.19 (0.07–0.57)	0.18 (0.06–0.52)	40.9 ± 1.3	0.10	37	$^{210}Pb_{ex}$ profile decreased exponentially with depth and the model fits well. ^{137}Cs activity was low and could not be used to validate rates.
12C	5	5	0.77	0.15 (0.06–0.37)	0.09 (0.04–0.22)	39.1 ± 1.4	0.37 ± 0.1	33	$^{210}Pb_{ex}$ profile decreased exponentially with depth, and model fits well. ^{137}Cs profile used to validate SAR.

These resemble average OC concentrations in Arctic shelf surface sediments, whereas the higher OC in core 12C is at the upper end of the range, typical of productive locations [45]. Core 12C also had the lowest $\delta^{13}C$ values (−22.0 ± 1.08‰ (n = 11), compared to −20.9 ± 0.52‰ (n = 16) in core 8 and −20.7 ± 0.31‰ (n = 8) in core Bell_10. The isotopic composition of OC ($\delta^{13}C$) varied linearly, with %OC reflecting more isotopically depleted values in the more OC-rich sediments ($r^2 = 0.62$, $p < 0.05$, Fig. S3b). These sedimentary organic carbon compositions could be explained by mixtures of marine organic matter (OM_{mar}) and terrigenous organic matter (OM_{terr}), considering the $\delta^{13}C$ signatures of OM_{mar} can range from enriched values above −18‰ in some macroalgae and ice algae to relatively depleted values of −20% to −26‰ in phytoplankton and very depleted values below −26‰ in terrestrial vascular plants [45–47]. The OC-rich core 12C likely reflects a productive marine setting in which pelagic sedimentation (i.e., the flux of phytoplankton-derived organic matter) dominates, whereas core 8 reflects a setting in which the main sources of sedimentary organic matter are isotopically enriched ice algae or kelp, and a strong supply of inorganic sediments from terrestrial erosion or over the tidal flats.

Across all the sediments, there was a strong positive linear relationship between OC and TN with a near-zero intercept for TN at %OC = 0 (Fig. S3a), indicating that inorganic nitrogen (which may be found bound to clays, for example [46]) is not significantly present. Core 12C had the highest TN (0.33 ± 0.08, n = 11) and lowest atomic carbon to nitrogen (C/N) ratios (7.73 ± 0.31, n = 11) among the cores, which could be explained by stronger OM_{mar} (weaker OM_{terr}) influence than the remaining cores. OC/TN ratios averaged 9.63 ± 0.71 (n = 10) in core 8, consistent with stronger OM_{terr} (weaker OM_{mar}) influence. It is also noteworthy that although cores Bell_10 and 12C had OC concentrations that decreased downcore as expected from in situ degradation and typically observed in Arctic shelf sediments cf. [44,48], the Koojesse Inlet cores 14, 4 and 8 had profiles in which OC increased below the surface to maximum values between 6 and 8 cm and then decreased with depth (Fig. S2). The subsurface peaks in OC imply a non-steady state organic matter supply within Koojesse Inlet. Increased mineral soil erosion due to development activities in Iqaluit cf. [22]. explains the unusual upcore decrease in OC in core 8.

3.3. Total mercury (THg)

THg concentrations ranged from 4.37 to 68.7 ng g^{-1} across the seven cores (Fig. 3a–c). Core 12C had the highest concentrations (33.8–68.7 ng g^{-1}) with a vertical profile in which THg increased towards the surface ($r^2 = 0.73$, $p < 0.05$). THg was lower in core Bell_10 (11.3–30.6 ng g^{-1}) but also increased upwards towards the surface ($r^2 = 0.86$, $p < 0.001$). These vertical trends were robust even if THg was normalized by dividing by OC content (Fig. 3d–f). THg is closely correlated with OC in both core Bell_10 and core 12C (r^2 = 0.89 and 0.77, respectively; Fig. S4). In contrast, THg concentrations in core 8 (11.1–17.1 ng g^{-1}) were not correlated with OC and did not increase toward the surface of the core. In core 8, THg peaked twice at depths of 25 cm (17.1 ng g^{-1}) and 7 cm (15.6 ng g^{-1}), the latter coinciding with peaks in concentration of several other inorganic elements, including arsenic (As), copper (Cu), iron (Fe), molybdenum (Mo), phosphorus (P), and zinc (Zn; Fig. 4). The low THg concentrations in core 8 likely reflect the high sedimentation rate in Koojesse Inlet. THg also was relatively low across all remaining cores collected from Koojesse Inlet (cores 4, 8, 14, 15, and 16), except for the 14 cm slice in core 4 (62.4 ng g^{-1}). THg concentrations of 1.93 ± 0.45 ng g^{-1} dw in sediment from intertidal regions of Koojesse Inlet [31] are about 2–13 fold lower than the concentrations in our sediment cores. These values suggest a very low background THg in the region's mineral soils/intertidal sediments, although the details of grain size and OC content of the intertidal sediments are unknown.

3.4. Polycyclic aromatic hydrocarbons (PAHs)

$\sum$PAHs ranged from 2.41 to 304 ng g^{-1} across the three cores (Fig. 5a–c). $\sum$PAHs in core 12C (2.41–18.9 ng g^{-1}) and core Bell_10 (2.86–25.1 ng g^{-1}) were independent of depth in the sediments. In contrast, $\sum$PAHs were high (50.3–304 ng g^{-1}) and increased upwards in core 8 ($r^2 = 0.63$, $p < 0.05$). Near-surface sediments from other cores in Koojesse Inlet (cores 4, 14, 15, and 16) had similar concentrations to core 8 (Fig. 5a). A total PAH concentration of 23.5 ng g^{-1} was previously reported in Frobisher Bay sediments [8].

Diagnostic ratios have previously been used to discriminate

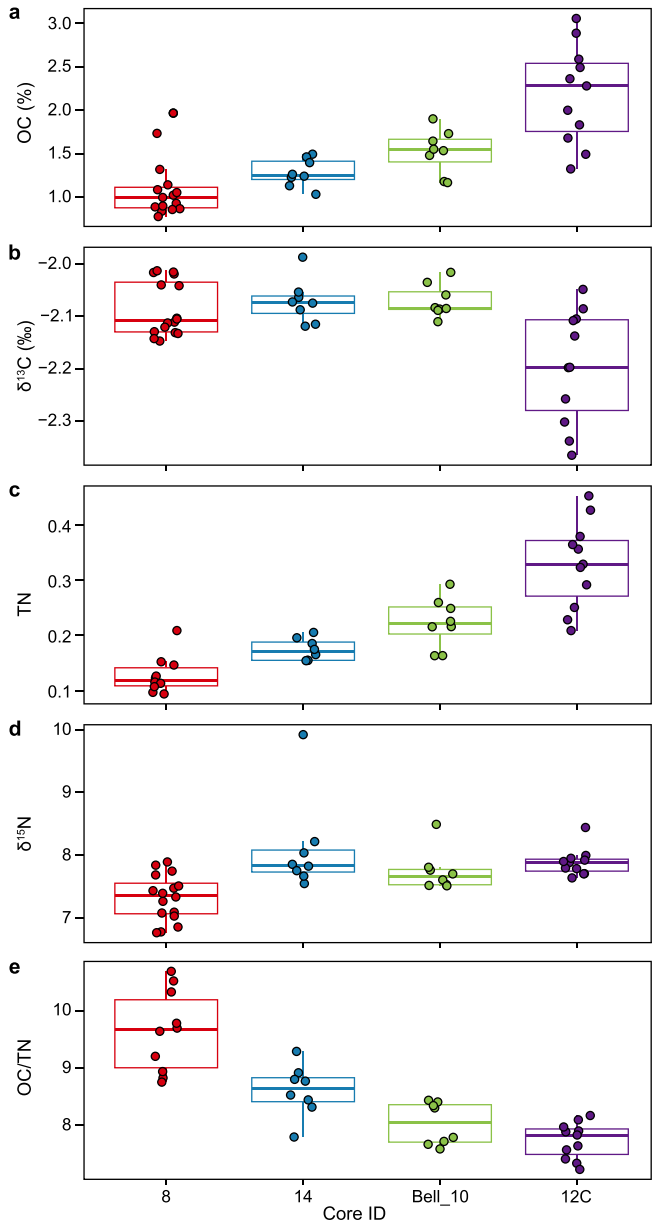

Fig. 2. Box plots of organic carbon (OC) (**a**), $\delta^{13}C$ (**b**), total nitrogen (TN) (**c**), $\delta^{15}N$ (**d**), and the ratio of organic carbon to total nitrogen (OC/TN) (**e**). Lower and upper box hinges correspond to the 25th and 75th percentiles. Medians are represented by a horizontal line in the box. Lower whiskers extend to the smallest value at most 1.5 × interquartile range (IQR) of the hinge. Upper whiskers extend to the largest value at most 1.5IQR of the hinge. Points beyond the whiskers are outlying data points.

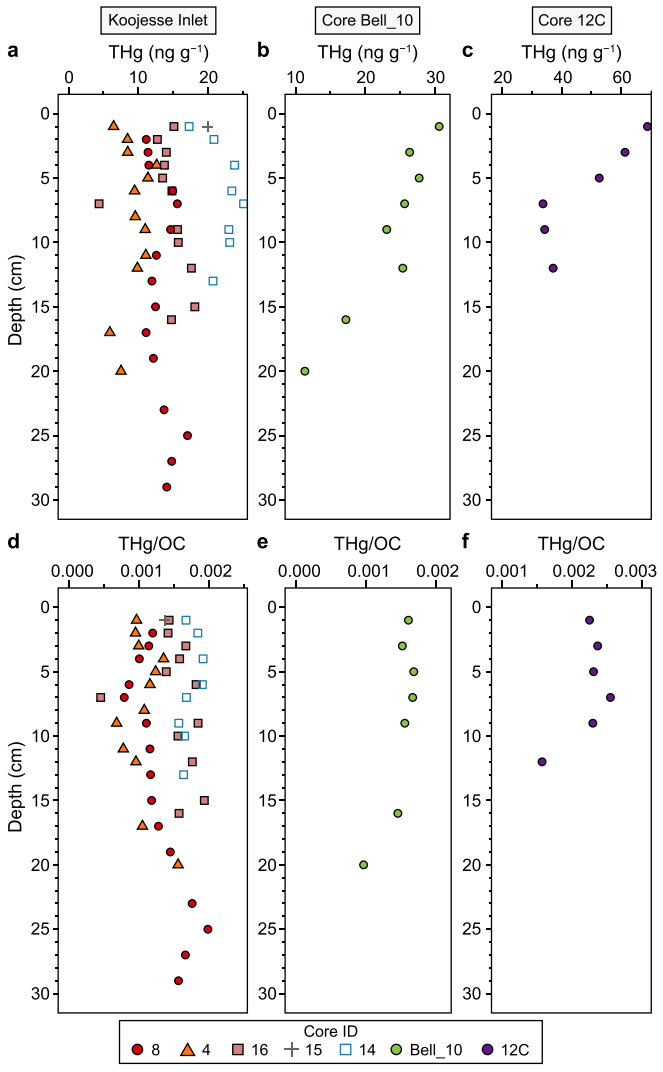

Fig. 3. **a**–**c**, Downcore profiles of total mercury (THg): Koojesse Inlet (**a**), Core Bell_10 (**b**), and Core 12C (**c**). **d**–**f**, organic carbon-normalized THg (THg/OC multiplied by 1000): Koojesse Inlet (**d**), Core Bell_10 (**e**), and Core 12C (**f**). THg is independent of OC in core 8 (see Fig. S4 for relationships). Data points correspond to the maximum depth in cm of each sediment slice analyzed for THg.

sources of PAHs (pyrogenic vs. petrogenic) in sediments [32,49]. Pyrogenic sources may include burning fossil fuels, coal or wood; petrogenic sources include materials derived from erosion of coal, peat, or bitumen deposits and active oil seeps [49]. In general, Fla/[Fla + Pyr] values below 0.4 indicate petrogenic origin, 0.4–0.5 suggests fossil fuel combustion, and greater than 0.5 implies biomass combustion [49]. For BaA/[BaA + Chr], values below 0.2 indicate petrogenic, 0.2–0.35 suggests mixed sources (i.e., either fossil fuel or biomass combustion), and greater than 0.35 implies pyrogenic [49]. In our study, all samples from core 8 were >0.5 for Fla/[Fla + Pyr], and >0.35 for BaA/[BaA + Chr], suggesting biomass combustion/pyrogenic origin. Samples from the other four cores in Koojesse Inlet (cores 4, 14, 15, 16) exhibited similar results (Fig. 5d,g). Three samples from core 15 were between 0.4 and 0.5 for Fla/[Fla + Pyr], and two were between 0.2 and 0.35 for BaA/[BaA + Chr], indicating either fossil fuel combustion or mixed sources. The predominance of pyrogenic sources in Koojesse sediments agrees with recent results of Corminboeuf et al. [32], who suggested that local anthropogenic activities, such as the use of diesel fuel or burning of waste, could be contributing to the pyrogenic PAHs found in the bay. PAH ratios were variable in the remaining cores indicating a range of possible PAH sources (Fig. 5e,f,h,i). For example, in core 12C, Fla/[Fla + Pyr] ratios were predominantly <0.4, indicating petrogenic origin, but BaA/[BaA + Chr] ratios were between 0.2 and 0.35 in three sections suggesting mixed sources (i.e., either fossil fuel or biomass combustion) but >0.35 in two sections suggesting pyrogenic sources.

3.5. Polychlorinated biphenyls (PCBs)

$\sum$PCBs of 0.18–0.67 ng g^{-1} in core 12C and 0.07–0.32 ng g^{-1} in core Bell_10 were very low compared to the range of

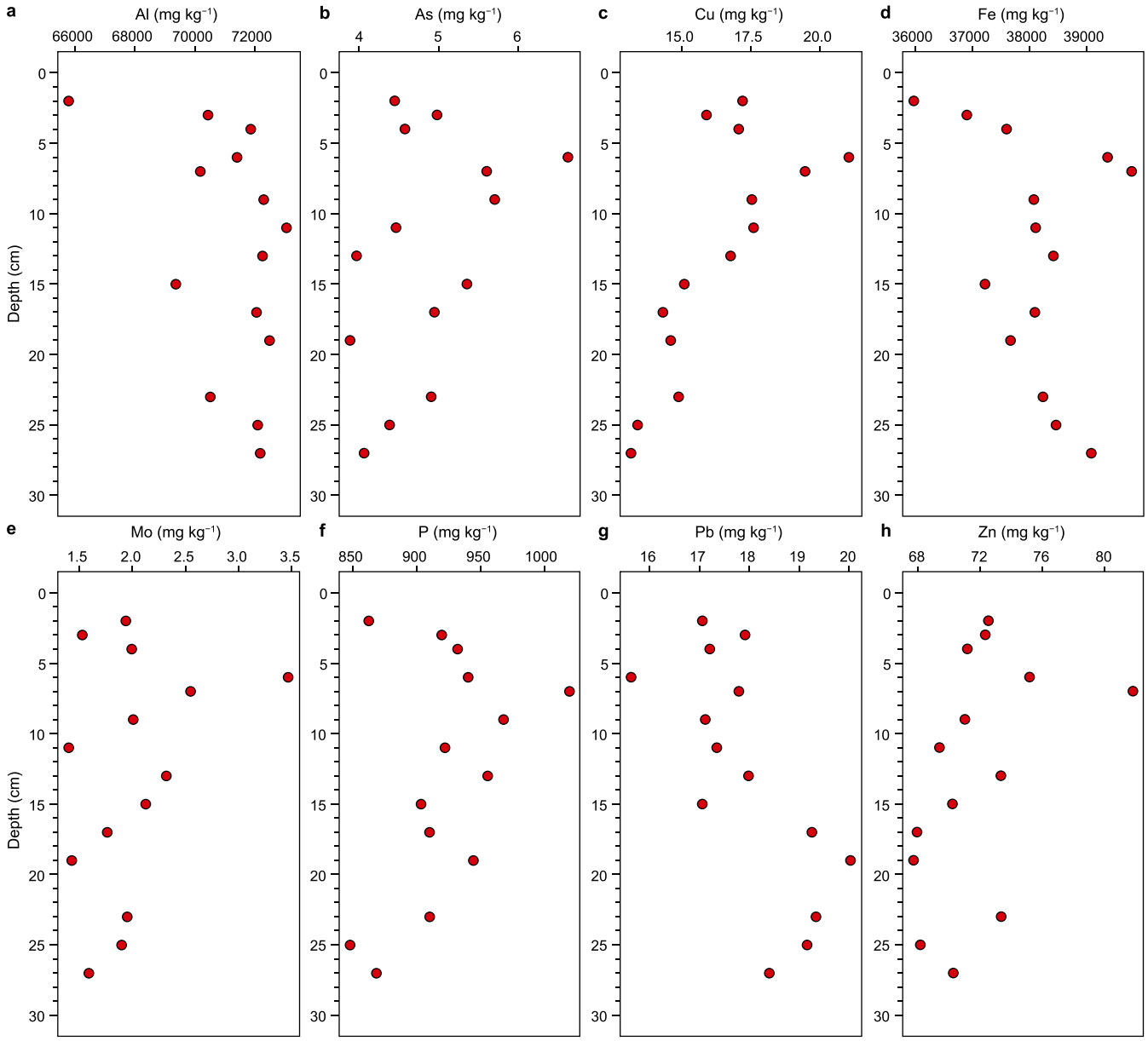

Fig. 4. Downcore profiles of the following major and trace elements in core 8: aluminum (Al) (**a**), arsenic (As) (**b**), copper (Cu) (**c**), iron (Fe) (**d**), molybdenum (Mo) (**e**), phosphorus (P) (**f**), lead (Pb) (**g**), and zinc (Zn) (**h**). Data points correspond to the maximum depth in cm of each sediment slice analyzed for elements.

concentrations of 10.1–46.7 ng g^{-1} in core 8 (Fig. 6). The vertical distributions of PCBs also were different among the cores. In both core 12C and core Bell_10, there was a significant upward increase in ∑PCBs ($r^2 = 0.84$, $p < 0.001$ and $r^2 = 0.57$, $p < 0.05$, respectively), which reflects low concentrations below 13 cm in core 12C and below 5 cm in core Bell_10 and higher constant concentrations in overlying sediment sections (Fig. 6b and c). In core 8, ∑PCBs were highest in sediment sections near the bottom of the core at depths between 23 and 27 cm and decreased upward following a roughly exponential shape (Fig. 6a). ∑PCBs in core 8 were 3.1- to 14.2-fold higher than previously reported concentrations from 1995 (47 congeners [8]). In contrast, ∑PCBs in cores Bell_10 and 12C were low compared to previous reports for marine sediments south of Koojesse Inlet (3.30 ng g^{-1} dry for 47 congeners [8]) and overlapped with the range of PCB concentrations (sum of 83 congeners; 0.040–0.150 ng g^{-1}) in surface sediments from Hudson Strait and Hudson Bay [50] as well as concentrations (sum of 51 congeners; 0.24 ng g^{-1}) in remote parts of Saglek Fjord, northern Labrador [9].

PCBs in cores Bell_10 and 12C were compositionally similar and included low and high chlorine content congeners. Core Bell_10 consisted primarily of congeners with 4, 5, or 6 chlorine atoms, while core 12C was dominated by congeners with 3, 4, 5, or 6 chlorines. The composition of core 8 was dominated by congeners with 6, 7 and 8 chlorine atoms. These compositional differences could explain the statistically significant differences in PCA factor scores for the three cores along the first component of the PCA (PC1; ANOVA, and Tukey HSD ($p < 0.001$), Fig. 7a). For the first component (PC1), which explained 65.5% of the variance, the congener loadings were negatively correlated with octanol-water partition coefficients (Log K_{ow}, Fig. 7b) meaning that a congener

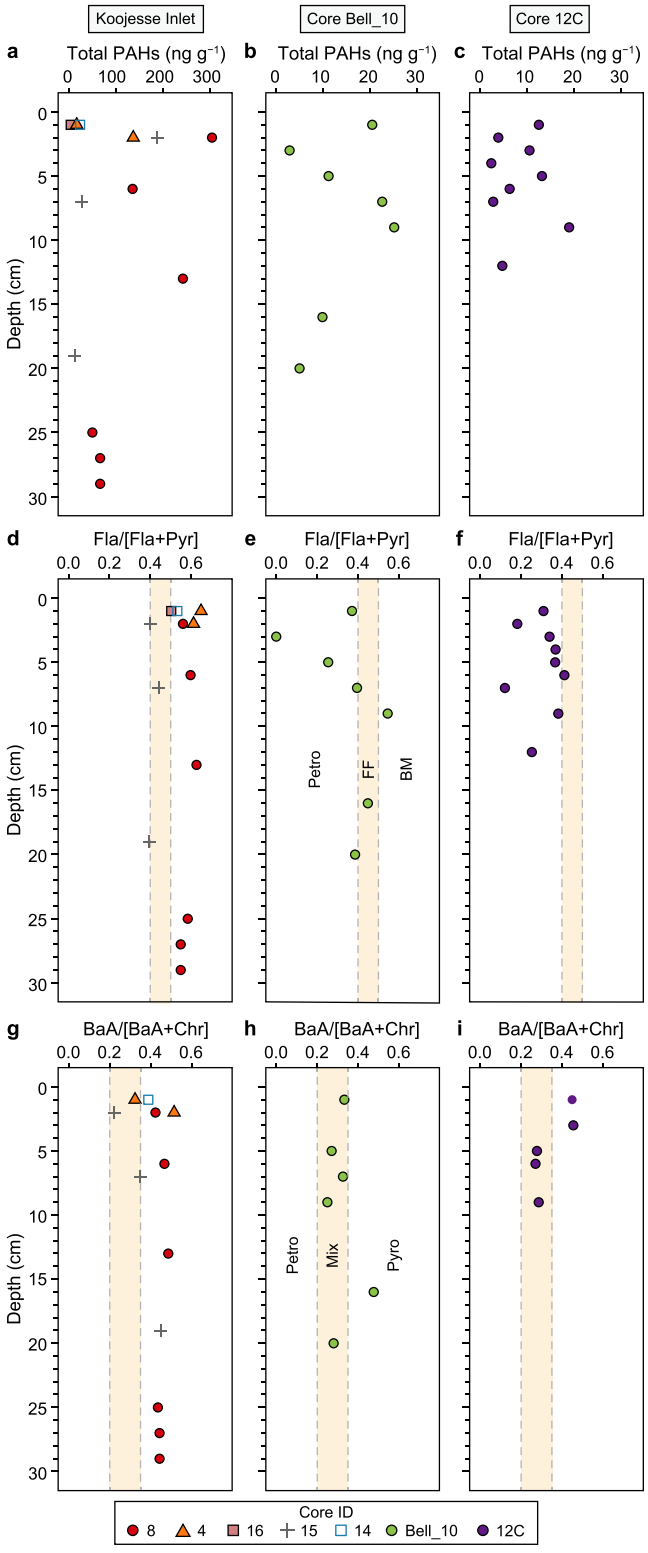

Fig. 5. **a**–**c**, Downcore profiles of total polycyclic aromatic hydrocarbon concentrations (∑PAHs): Koojesse Inlet (**a**), Core Bell_10 (**b**), and Core 12C (**c**). **d**–**f**, Diagnostic ratios for PAHs fluoranthene (Fla) and pyrene (Pyr): Koojesse Inlet (**d**), Core Bell_10 (**e**), and Core 12C (**f**). **g**–**i**, benz(*a*)anthracene (BaA) and chrysene (Chr): Koojesse Inlet (**g**), Core Bell_10 (**h**), and Core 12C (**i**). Vertical dashed lines show cutoff values for the ratios. For Fla/[Fla + Pyr], <0.4 is petrogenic (Petro), 0.4–0.5 is fossil fuel combustion (FF), and >0.5 is biomass combustion (BM). For BaA/[BaA + Chr], <0.2 is petrogenic (Petro), 0.2–0.35 is mixed sources (Mix), and >0.35 is pyrogenic (Pyro). Samples with zero values for either ratio are not included in this figure. Data points correspond to the maximum depth in cm of each sediment slice analyzed for PAHs.

composition dominated by congeners with higher Log K_{ow} values, many of which have high degrees of chlorination, leads to negative scores and projection to the left side of the plot. The projection of core 12C on the far right side of the scores plot is explained by higher contributions of congeners with low degrees of chlorination relative to the other two cores. In contrast, the projection of core 8 on the far left side of the plot is explained by higher contributions of congeners with high degrees of chlorination. Core 8 plotted further to the left in Fig. 7a than the highly chlorinated Aroclor 1260 industrial mixture that was used at the military site in Iqaluit in the 1950s and detected at the highest concentration in the sediments south of Koojesse Inlet [8]. Core Bell_10 was projected into approximately the centre of the plot along PC1, which may be explained by contributions of congeners with both high and low degrees of chlorination relative to cores 12C and 8. In general, heavier congeners had lower/negative factor loadings, and lighter congeners had higher/positive loadings on PC1. The following congeners had the ten lowest factor loadings on PC1 and were thus influential in projecting core 8 far to the left: 180/193, 194, 187, 176, 179, 141, 147/149, 129/138/163, 174, and 172. The following congeners had the ten highest factor loadings on PC1: 64, 22, 86/87/97/109/119/125, 61/70/74/76, 31, 45/051, 56, 44/47/65, 20/28, 49/69.

The second component of the PCA (PC2) explained only an additional 6.4% of the variation in PCB composition. Cores Bell_10 and 12C get separated along PC2 with high and low scores, respectively, while core 8 lies more or less in the middle with scores not significantly different from 12C (Tukey HSD, $p < 0.01$). PC2 scores did not change significantly with depth in cores 8 and Bell_10 and were only marginally lower in the deep slices of core 12C ($p < 0.10$). PC2 congener loadings were not correlated with Log K_{ow} or degree of chlorination. Rather, subtle congener-specific differences between cores Bell_10 and 12C are reflected in the PC2 scores.

3.6. Per and polyfluoroalkyl substances (PFASs)

∑PFASs ranged from 0.116 to 1.00 ng g^{-1} and increased upwards in core 12C ($r^2 = 0.72$, $p < 0.001$). In core Bell_10, ∑PFASs ranged from 0.047 to 0.427 ng g^{-1}, and increased upwards ($r^2 = 0.52$, $p < 0.01$). Both core Bell_10 and core 12C had an exponentially increasing upwards trend in ∑PFASs, albeit with one pronounced peak at 12 cm (0.34 ng g^{-1}) in core Bell_10. Concentrations in the top 10 cm of cores 12C and Bell_10 corresponded to 0.39 ± 0.30 and 0.22 ± 0.11 ng g^{-1} ΣPFASs (mean ± SD), respectively. ∑PFASs in core 8 ranged from 0.060 to 1.32 ng g^{-1}, and its concentration-depth profile diverged from cores Bell_10 and 12C. The maximum concentration in core 8 occurred at 11–13 cm (1.32 ng g^{-1}) depth. Using the sedimentation and mixing rates in this core and the advective-diffusive model in MATLAB [51], a similar peak can be reproduced by an input pulse during the 1990s. Additional information on this transient tracer method is provided in the SI. After log normalizing (log base 10), ∑PFASs in the upper 20 cm of core 8 showed little variation aside from this depth (Fig. 8). ∑PFASs in core 8 remained slightly lower than in sediments from the North and Baltic seas [52], but were similar to those in sediments from the Bering Sea and the western Arctic [53].

Based on the major PFAS congener classes: perfluorocarboxylic acids (PFCAs), perfluorosulfonic acids (PFSAs) and fluorotelomer carboxylic acids (FTCAs), all three cores were dominated by PFCAs, followed by PFSAs (Fig. 9). FTCA compounds were only consistently detected in core 8. The composition of PFCAs in cores Bell_10 and 12C were similar, consisting of chain lengths from 8 to 11 carbons: PFOA, PFNA, PFDA, and PFUnDA. While these PFCAs were also present in core 8, the PFSAs were particularly pronounced in this core, particularly PFOS and PFDS. Compositional variation extended

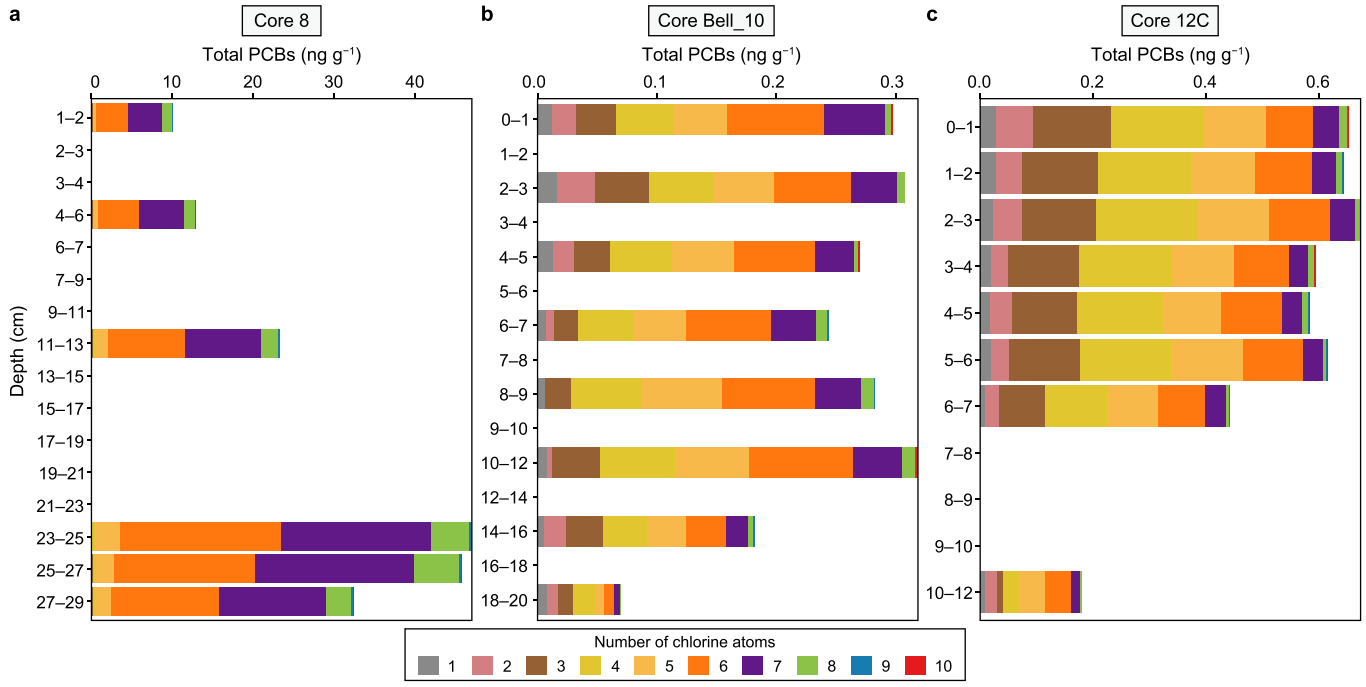

Fig. 6. Downcore profiles of total polychlorinated biphenyls concentrations (∑PCBs), grouped by degree of chlorination: Core 8 (**a**), Core Bell_10 (**b**), and Core 12C (**c**). Data points are represented by the range in cm of the depth of the sediment slices analyzed for PCBs.

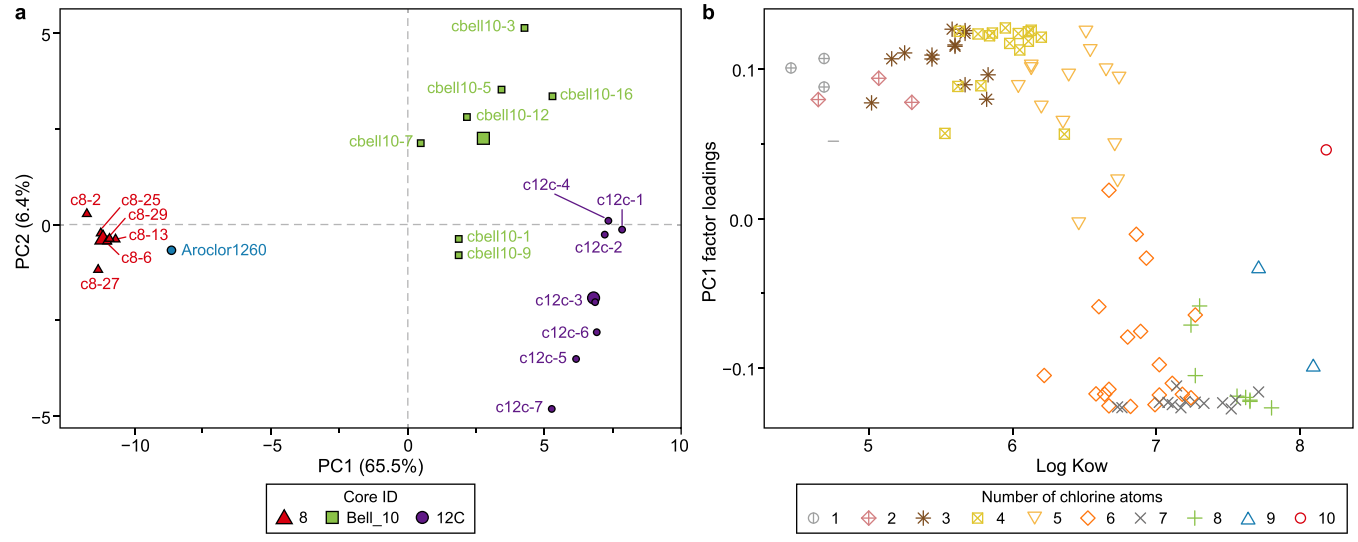

Fig. 7. **a**, Principal Component Analysis (PCA) of polychlorinated biphenyls (PCBs). Factor scores plot with the projection of industrial mixture Aroclor 1260. Scores (samples) are labelled with the core name (c8 = core 8, cbell10 = core Bell_10, and c12c = core 12C) followed by the maximum depth of the sediment slice in cm. **b**, Factor loadings for principal component 1 (PC1) vs. the octanol-water partition coefficients (Log K_{OW}) for the PCB congeners. PC1 and PC2 explains 65.5% and 6.4% of the variance, respectively.

throughout core 8, despite the low variation in total PFAS concentration. For example, PFSAs were dominant in the 17–19 and 19–21 cm slices, whereas PFCAs were dominant in slices 7–9, 6–7, and especially 4–6 cm (Fig. 9; see also Fig. S5, which shows the relative contributions of individual compounds).

4. Discussion

4.1. Evidence for local contaminant inputs near Iqaluit

Although shelf sediments contain unique records of contaminant inputs depending on sedimentation rates, mixing rates, and fluxes of organic matter of different origins cf. [37], comparison of the contaminant concentration ranges in Koojesse Inlet sediments, other Frobisher Bay cores, and previously reported Arctic sediments indicate local inputs of PCBs, PAHs, and PFASs to Koojesse Inlet sediments in addition to ubiquitous inputs from LRT (Table 3). Levels of PCBs in Koojesse Inlet semi-pelagic sediments were several-fold higher than in other Arctic shelf sediments. They were 3 to 14-fold higher than concentrations previously measured south of Koojesse Inlet in 1994 [8]. PAHs were up to 13-fold higher in Koojesse Inlet sediments than in Frobisher Bay in 1994 [8] but

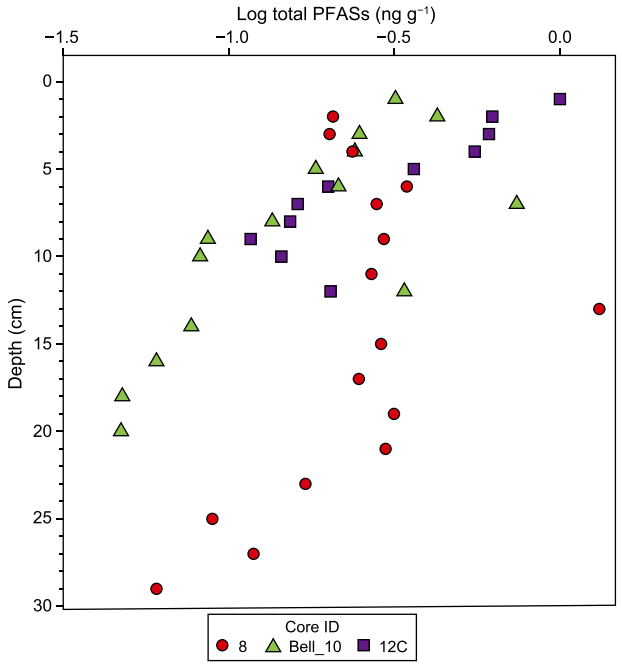

Fig. 8. Downcore profiles of log-normalized (log base 10) total per and polyfluoroalkyl substances concentrations (∑PFASs) in cores 8, Bell_10, and 12C. Data points correspond to the maximum depth in cm of each sediment slice analyzed for PFASs.

were similar to concentrations in marine sediments from the Canadian Arctic Archipelago measured more recently [32]. At their peak, the PFASs also exhibited maximum concentrations in Koojesse Inlet sediments, although these concentrations remained below those observed in the North and Baltic seas [52].

Our best record of the local contaminant inputs into Koojesse Inlet exists in core 8, which had a clear subsurface ^{137}Cs peak below 25 cm (Fig. S1). Whereas interpretation of the ^{210}Pb profile alone would tend to cause an overestimate of the sedimentation rate because of downward mixing, the peak in ^{137}Cs near the bottom of the core confirms that the sedimentation rate is 0.5 cm yr^{-1}, at the lower limit of the range of rates derived from ^{210}Pb. Within the ca. 20-year intrinsic time resolution of core 8 (Table 2), the bottom few slices of the core that contain the PCB peak can be tied to deposition during the 1950–1960s. In 1942, the construction of a US Air Force Strategic Air Command base began in the location of the current airport in Iqaluit [26]. The site was managed by the Canadian Air Force between 1946 and 1950 [8]; however, from 1951 to 1963, US Air Force activities included the construction of Upper Base, a Pole Vault radar station at the summit above Iqaluit [8]. The intention of building this large military airfield was to have a refuelling base for short-range military aircraft en route from America to Great Britain [26]. Based on the time frame of the peak in PCBs and the highly chlorinated composition of PCB congeners in these slices, we propose that the Aroclor 1260 used in Iqaluit in these initial years reached the coastal environment, possibly through erosion of contaminated soil and transport via the stream that runs near the Upper Base, the military sites near the airport, and the industrial sites around the airport, and into Koojesse Inlet. Civilian and military dump sites located near the sea shore around Iqaluit (West 40, North 40, and Apex dump) [8] also may have affected the concentrations in the sediments.

Although the concentration range for THg in Koojesse Inlet sediments is not different from that in typical Arctic sediments (Table 3), a spike in THg at 25 cm occurred at the same time as the peak in PCBs, which could indicate that local sources of Hg in Iqaluit increased when the military and civilian infrastructures were being built and/or in operation. Hg was present in older thermometers, fluorescent light bulbs, and electrical switches. Furthermore, local activities like construction may have mobilized Hg from the terrestrial to coastal environments. The historical input of THg certainly was minor compared to the PCB input, and the 25 cm peak

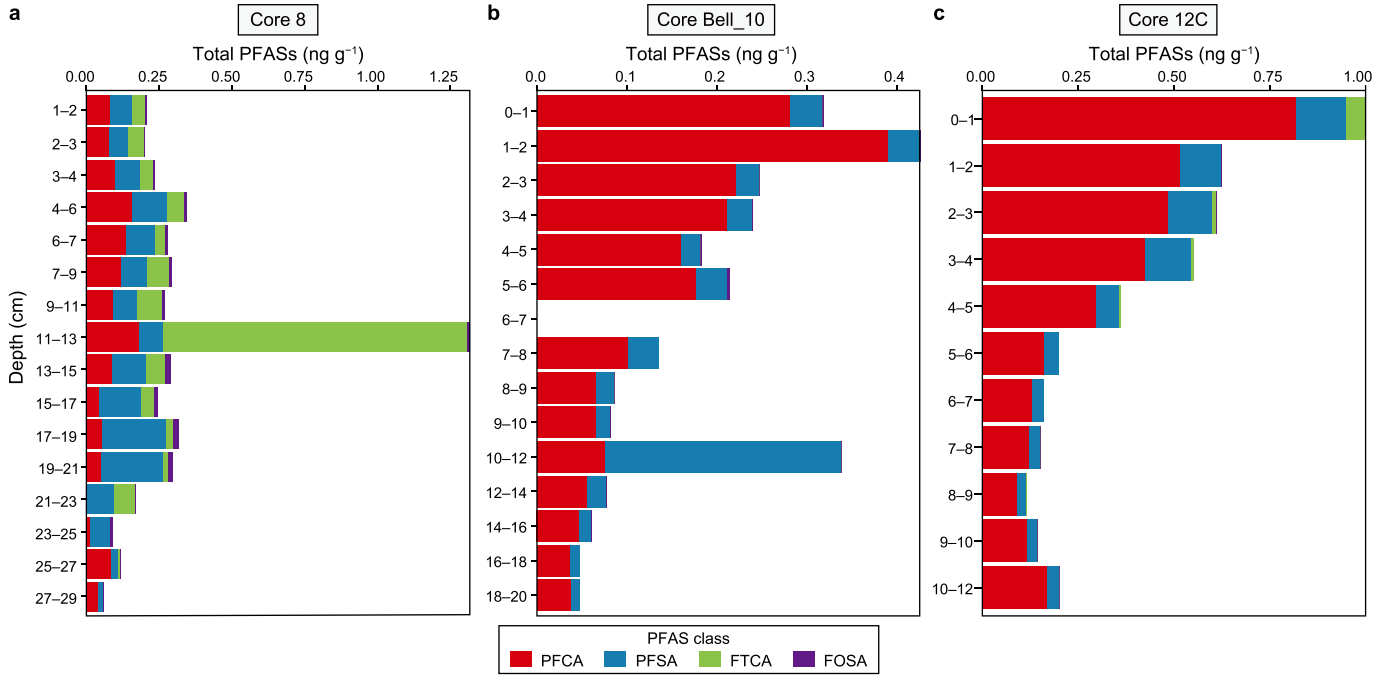

Fig. 9. Downcore concentrations of major per and polyfluoroalkyl substances (PFASs) congener classes: perfluorocarboxylic acids (PFCAs), perfluorosulfonic acids (PFSAs), fluorotelomer carboxylic acids (FTCAs), and FOSA: Core 8 (**a**), Core Bell_10 (**b**), and Core 12C (**c**). Data points are represented by the range in cm of the depth of the sediment slices analyzed for PFASs.

Table 3
Results for contaminants measured in sediment cores from Frobisher Bay, Nunavut, compared to previously reported values in Arctic sediments.

Contaminant class	Concentration in Frobisher Bay, NU	Summary of previously reported values	Reference
Elements	Cores 4, 8, 16: As 3.88–12.06 mg kg^{-1} Cu 6.53–12.07 mg kg^{-1} Pb 13.73–20.03 mg kg^{-1} Zn 47.73–81.81 mg kg^{-1}	Baffin region, NU (1994) As 0.3–3.5 μg g^{-1} Cu < 3.0–27 μg g^{-1} Pb < 10 μg g^{-1} Zn 8.1–103 μg g^{-1} (marine) South of Koojesse Inlet, NU (1994) As 0.3 μg g^{-1} Cu 15–27 μg g^{-1} Pb < 10 μg g^{-1} Zn 100–103 μg g^{-1} (marine)	[8] [8]
THg	Cores 4, 8, 14, 15, 16: 4.37–62.37 ng g^{-1} Core Bell_10: 11.34–30.62 ng g^{-1} Core 12C: 33.76–68.74 ng g^{-1}	Frobisher Bay, NU (2019) 1.93 ± 0.45 ng g^{-1} dw (THg, intertidal marine) Hudson Bay, Canada (2005) 8–58 ng g^{-1} (Hg, marine) Baffin region, NU (1994) <0.2 μg g^{-1} (inorganic Hg, marine) South of Koojesse Inlet, NU (1994) <0.2 μg g^{-1} (inorganic Hg, marine)	[31] [58] [8] [8]
PAHs reported as a sum of 15 compounds	Cores 4, 8, 14, 15, 16: 4.38–304.20 ng g^{-1} Core Bell_10: 2.86–74.79 ng g^{-1} Core 12C: 2.41–18.94 ng g^{-1}	Canadian Arctic Archipelago (2016–2019) 7.8–247.7 ng g^{-1} dw (16 US EPA priority PAHs, marine) 22.1–108.8 ng g^{-1} dw (16 US EPA priority PAHs, terrestrial) Baffin region, NU (1994) 7.5–12 ng g^{-1} (total LPAH, marine) 5.0–18 ng g^{-1} (total HPAH, marine) Frobisher Bay, NU (1994) 7.5 ng g^{-1} (total LPAH, marine) 16 ng g^{-1} (total HPAH, marine)	[32] [8] [8]
PCBs reported as a sum of 161 individual or co-eluting congeners	Core 8: 10.1–47.0 ng g^{-1} Core Bell_10: 0.07–0.32 ng g^{-1} Core 12C: 0.18–0.67 ng g^{-1}	Hudson Bay, Canada (2005) 40–150 pg g^{-1} dw (sum congeners, marine) Saglek Bay, Labrador (1997–1999) 0.24–62 000 ng g^{-1} dw (55 congeners, marine) Baffin region, NU (1994) 0.023–3.3 ng g^{-1} (47 congeners, marine) South of Koojesse Inlet, NU (1994) 3.30 ng g^{-1} (47 congeners, marine) Cambridge Bay, NWT (1991–1993) 0.14–45 ng g^{-1} dry (47 congeners, marine) Queen Maud Gulf and Wellington Bay, Victoria Island, NWT (1991–1993) 0.052–0.44 ng g^{-1} dry (47 congeners, marine)	[50] [9] [8] [8] [66] [66]
PFASs reported as a sum of 18 compounds	Core 8: 0.06–1.32 ng g^{-1} Core 12C: 0.116–1.00 ng g^{-1} Core Bell_10: 0.06–1.32 ng g^{-1}	German Bight, German Baltic Sea, North Sea, the Skagerrak and Kattegat (2016–2017) 0.018–2.6 ng g^{-1} dw (29 compounds, marine) Bering Sea and western Arctic, mainly Chukchi Sea (2014 and 2016) 0.06–1.73 ng g^{-1} dw (9 compounds, marine) Lake Hazen, NU (2012) 0.006–0.161 ng g^{-1} dw (13 compounds, terrestrial) Lake B35, NU (2009) 0.044–1.52 ng g^{-1} dw (7 compounds, terrestrial)	[52] [53] [14] [14]

in THg is not much larger than the peak in the top 10 cm of the core.

PAHs were detected in the lower slices of core 8 but not at high levels, and indeed the PAH concentrations increased up to 10-fold toward the surface. They had a pyrogenic signature in all slices. This signature and the upward increase may be explained by fossil fuel combustion in and around Iqaluit (electricity, heating, and transportation sectors), which has increased with an increasing urban population since its establishment in 1942. The burning of waste may also contribute to this trend. The results support Corminboeuf et al.'s [32] conclusion that local combustion sources affect PAH concentrations in Koojesse Inlet sediments.

PFASs were also detected throughout most sections of core 8, with consistent detection between 1 and 21 cm (Fig. 9). This corresponds to deposition between the 1980s and 2000s, which is consistent with emissions trends of PFASs as well as sedimentation and mixing rates in the core (Fig. 10). Deposition between the 1980s and 2000s makes sense both with the sedimentation and mixing rates in the core and the emission trends for PFASs (Fig. 10). Based on the shifting compositional patterns of PFASs in core 8, the sources to Koojesse Inlet have evolved during the past 30 years. The PFOS + PFDS prominence at 15–21 cm may be explained by legacy aqueous film-forming foam (AFFF) usage at the airport or other fuel-storage facility agents. AFFF was used to extinguish hydrocarbon-fuel fires, and their repeated usage led to AFFF contamination at many airports and military sites across North America [54]. A second terminal was built at the Iqaluit airfield in 1987, and it remained a kind of strategic hub for the military, providing backup fuelling for transatlantic flights. The upper reaches of core 8 have more FTCAs, which are not seen in the other two cores. This may be explained by the airport switching its AFFF chemistry after the phase-out of PFOS formulations towards more novel fluorotelomer chemistry. FTCAs are intermediates in the degradation of fluorotelomer alcohols and other fluorotelomer-based substances to PFCAs, and FTCAs are considered more toxic than the PFCAs themselves [55]. More research is needed to discern the transport mechanism of FTCAs (or FTCA-precursors) from

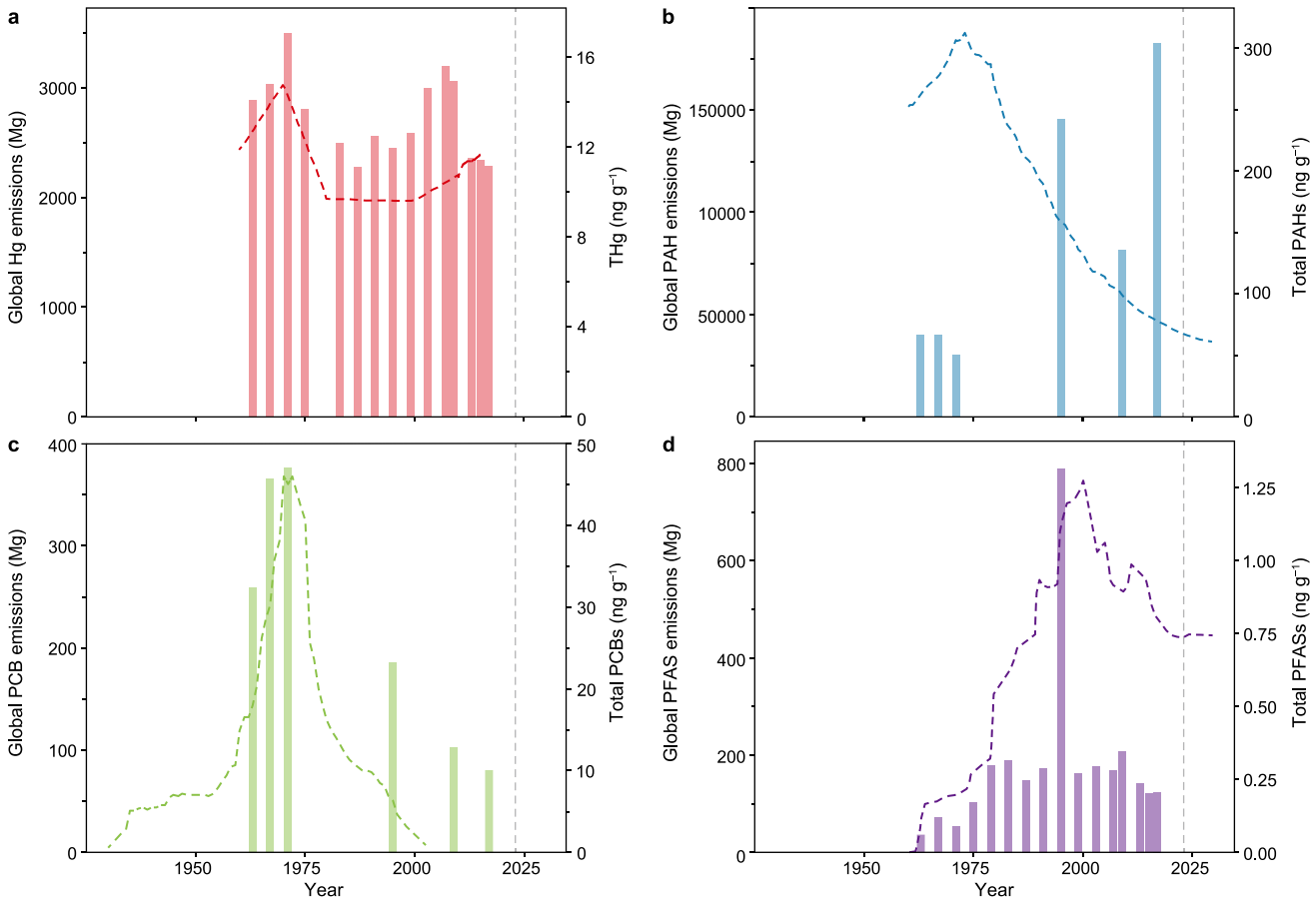

Fig. 10. Historical global emissions of mercury (Hg) (**a**), polycyclic aromatic hydrocarbons (PAHs) (**b**), polychlorinated biphenyls (PCBs) (**c**), and per and polyfluoroalkyl substances (PFASs) (**c**), represented with dashed lines. Total contaminant concentrations in core 8 are represented by bars. Annual global Hg emissions from 1960 to 2015 were redrawn from Ref. [61]. Decadal trends before 2010 originally from Ref. [62]. PAH emissions from 1960 to 2030 for developed countries, redrawn from Ref. [63]. Post-2010 data are future time trend simulations. PCB emissions of sum 22 PCBs from 1930 to 2000, redrawn from Ref. [64]. PFAS estimated total global annual emissions of C4–C14 PFCAs from 1951 to 2030 (higher production scenario). Redrawn from Ref. [15], originally from Ref. [65].

proximal use in the airport to sediment in the bay, but runoff and groundwater transport are possible.

In the top half of core 8 (1–13 cm), the levels of PCBs exhibit a decline, with the lowest concentrations observed at the surface. There were no major changes in congener composition, suggesting that sources have remained the same. However, either the input rate has decreased, or the contaminated material is being diluted by more uncontaminated sediment. The clean-up of the military site in the 1990s and 2010s could explain the decrease in PCB concentrations. However, since they are still being detected in the top 2 cm of the sediments at high concentrations relative to cores Bell_10 and 12C, we propose that PCBs are still reaching Koojesse Inlet from local land-based sources and/or being remobilized and redistributed within the local marine environment. Surficial PCB distribution throughout Koojesse Inlet was not delineated.

Another feature in the top half of core 8 is a second peak in THg at 7 cm, co-located with a peak in OC. This is notable because there is no correlation between THg and OC in core 8. Thus, the 7-cm peak in both THg and OC is interpreted as reflecting THg introduction (or at least increased THg capture in sediments) with wastewater inputs. An increase in PAHs is observed up the core, and the pyrogenic signature remains in the 7 cm and surrounding slices, but there is nothing novel about the PAH signature at 7 cm. If the elevated THg peak resulted from a stronger biological pump, we would expect to observe a corresponding influence on affecting the PAH signal at this depth, as indicated by Ref. [18].

After the 11–13 cm slice, further up in the core, FTCA levels decrease, but PFCAs and PFSAs, particularly PFOS, continue to be detected. Two long-chain PFCAs, PFDA and PFNA, were highly correlated in core 8 and the remaining cores (Fig. S6). The consistency in the correlation suggests that LRT, likely atmospheric transport and deposition, were sources. Previous research has shown that the correlation between PFCAs that have x and $x+1$ carbons in remote environments, such as the Arctic supports the mechanism of LRT of volatile fluorotelomer precursors and atmospheric oxidation [56]. For example, oxidation of 8:2 fluorotelomer results in PFOA and PFNA in a 1:1 ratio [16]. The presence of PFCAs in upper sediment sections may be explained by continued LRT. Because PFSAs were also present at the surface, we infer that inputs continue from local sources in Iqaluit. FTCA was not detected at the surface, implying that the influence of the airport has decreased.

4.2. Evidence for long-range transport in Core 12C

Core 12C was sampled from outer Frobisher Bay, about 92 km from Iqaluit, and thus further away from potential local sources of contaminants than other cores. The vertical profiles of PCBs and THg in core 12C may be explained by natural processes and contaminant inputs associated with long-range transport. Although ∑PCBs increased significantly upcore in core 12C (Fig. 6), its

congener composition had a lower molecular weight. It was less chlorinated than other cores (Fig. 7a), typical of the PCBs deposited in Arctic sediments after having undergone LRT. For example, "background" marine sediments collected in the Baffin region in the 1990s contained predominantly less-chlorinated congeners 31, 28, 52, 49, 44, 74/94, 66/80/95 and 90/101 [8]. Many of the same compounds contributed strongly to the ∑PCBs in core 12C. The upward increase of PCBs in core 12C (Fig. 6) resembles the vertical PCB profiles in sediment cores from Hudson Bay and Hudson Strait, where LRT is the main PCB source [50]. Model simulations demonstrated that those PCB profiles were consistent with the assumption of PCB deposition starting between 1930 and 1950, peaking between 1965 and 1985, and decreasing thereafter. Global emissions of PCBs peaked before 1975 (Fig. 10). Five of the six cores from Hudson Bay and Hudson Strait had slightly but not significantly lower PCB concentrations in the surface sediment sections compared to the underlying sediment sections. One core had slightly (not significantly) higher concentrations in the surface section (see Fig. S1 in Ref. [50]). In core 12C, the top two sections have similar concentrations that are perhaps slightly lower than the concentration in the third section, considering the good repeatability of the analysis (Fig. 6). However, with a 33-year time resolution in core 12C and worldwide production of PCBs thought to have ended only in 1993 cf. [57], a decrease in PCB concentration in the surface section of the core may not be observed. Climate change effects may also contribute to maintaining LRT PCB inputs in recent years through increased volatilization in source areas or enhanced scavenging on phytoplankton with a longer ice-free season and increased phytoplankton productivity.

The vertical profile of THg in core 12C is also consistent with long-range transport when considering the relationship between Hg deposition, particle scavenging, and particle composition [58]. The positive relationship between THg and OC within these sediments, with a positive y-intercept of 4.24 ng g^{-1} at OC = 0, implies that THg is OC-bound. Considering the high OC and OM_{mar} signature in core 12C, we attribute the THg-OC relationship to particle scavenging in the water column, specifically the scavenging of THg on phytoplankton-derived marine organic matter. In sediments dominated by pelagic sedimentation and little inorganic sediment deposition, the distribution of OC in the sediments exerts a major control on the Hg profile.

In terms of PAHs, concentrations were generally low in core 12C and did not increase or decrease significantly up the core (Fig. 5c). Fla/[Fla + Pyr] diagnostic ratios showed that most slices exhibited a petrogenic PAH signature (Fig. 5c). However, the BaA/[BaA + Chr] ratios (for slices with non-zero concentrations) were quite variable, with some slices showing mixed sources while others showing pyrogenic. Considering the ship traffic passing in and out of Frobisher Bay for many decades and the fossil fuel combustion in Iqaluit, it is possible that air pollution originating within the Canadian Arctic and passing ships has had some influence on the PAH composition. Nevertheless, the observed levels of PAHs and petrogenic ratios are generally primarily attributable to natural sedimentary processes.

The upward increase in PFASs in this core was likely the result of LRT and shows the restricted amount of mixing on the surface of core 12C. Like core 8, there was a correlation between PFDA and PFNA in this core (Fig. S6c), providing evidence of LRT.

4.3. Evidence for both local and long-range transport in Core Bell_10

Comparison of core Bell_10 to other cores in Frobisher Bay indicates that the sediments in inner Frobisher Bay, further away from Iqaluit, are still influenced by local sources of PCBs and PFASs from the city in addition to LRT of contaminants. Although PCB concentrations in core Bell_10 were lower than in core 8, we propose that local sources in Iqaluit still influence the levels found in inner Frobisher Bay. In general, the composition of PCBs in core Bell_10 contains congeners with lighter molecular weights and fewer chlorine atoms than in core 8. However, there were also statistical differences in PCB composition between cores Bell_10 and 12C. Indeed, cores Bell_10 and 12C were different from each other on both PC1 and PC2 (Fig. 7a). On PC1, the significantly lower scores of core Bell_10 are associated with an increased relative abundance of highly chlorinated compounds that we do not expect to be delivered by LRT. Evidence of short-range transport of PCBs to soils, terrestrial plants, and marine environments within 20 km of a radar site in the Canadian Arctic has been observed previously [59,60]. Core Bell_10 was sampled 9.21 km away from the Iqaluit sewage lagoon; thus, it is plausible that PCBs could be reaching areas further away from Iqaluit but still within the inner bay. ∑PCBs increased upwards in core Bell_10 and remained similar in composition across all slices, suggesting that this local influence continues to be an important source of the sediment in this region.

OC increased upwards in core Bell_10, in a similar shape to the increasing THg concentrations. Fig. S4b shows a positive linear relationship between OC and THg in core Bell_10. The increase in THg could be related to increased particle scavenging in the water column. Diagnostic ratios of PAHs show that the PAHs in core Bell_10 came from various possible sources, both from petrogenic and pyrogenic origin. This result is consistent with the interpretation of some short-range transport of contaminants from the Iqaluit area. Ship traffic over the site also may contribute to pyrogenic PAH inputs. Small spills of hydrocarbons in Frobisher Bay would not be unexpected given the ship traffic and fuel transfer activities that have been conducted for many decades.

The composition of PFASs in core Bell_10 shows a peak in ∑PFASs at 10–12 cm, primarily influenced by an increase in PFOS. The peak in PFOS could be related to the military and major airfield presence in Iqaluit. PFOS and other PFSAs were observed throughout core 8; therefore, the influence of these PFASs may have spread beyond the region closest to Iqaluit. However, like the other two cores, correlations between PFDA and PFNA indicated that LRT was also an important source. Aside from the spike in PFOS, the PFAS composition in core Bell_10 more closely resembled that of core 12C.

5. Conclusion

This study of contaminant profiles in seven dated marine sediment cores from Koojesse Inlet, inner and outer Frobisher Bay, Nunavut, provides evidence for the importance of both long-range contaminant sources and local inputs in Arctic environments. Sediments collected 1.8 km away from Iqaluit received inputs of PCBs, THg, PAHs, and PFASs primarily originating from activities in and around Iqaluit. PCB contamination associated with the historic civilian and military activity in Iqaluit continues to represent a source of PCBs to coastal sediments, albeit reduced from a factor of at least 4*X* from its peak in the ~1960s. Records of THg in sediment suggest that although concentrations were not different from other areas of the Arctic, inputs were connected to local civilian and military activities and were potentially mobilized by local activities such as construction. PAH concentrations increased in recent sediments, likely reflecting increased fossil fuel burning for transportation (ships and airplanes), heating and electricity associated with the rapid population growth of Iqaluit in recent decades and northern development. In addition to fossil fuel burning, burning waste in Iqaluit may have contributed to the observed PAH levels. The dominant PFASs observed in this core were associated with

airport and military activities. Sediments located 92 km away from Iqaluit do not show evidence of direction contamination from local anthropogenic sources, but rather records suggest contaminants sourced from long-range transport. The input from local contamination is directly proportional to the distance separating the sample and the focal point of contamination in northern Koojesse Inlet. In sediment collected 9.2 km away from Iqaluit, inputs from both long-range transport and local sources contributed to the contaminant concentrations observed. PCB, PAH, and PFAS compositions indicated that local contaminants were delivered to the sediments of inner Frobisher Bay, further away from Iqaluit. These results highlight that even after the clean-up of legacy military sites, there remains an impact on the environment for many decades. As human activities escalate in the Arctic, comprehensive investigations into contaminant levels and prospective ecological ramifications hold paramount importance for evaluating risks within regions of significance for traditional food harvesting.

CRediT authorship contribution statement

Meaghan C. Bartley: Formal Analysis, Data Curation, Writing - Original Draft, Visualization. **Tommy Tremblay:** Formal Analysis, Investigation, Writing - Review & Editing, Visualization. **Amila O. De Silva:** Investigation, Writing - Review & Editing. **C. Michelle Kamula:** Conceptualization, Investigation, Writing - Review & Editing. **Stephen Ciastek:** Investigation, Writing - Review & Editing. **Zou Zou A. Kuzyk:** Conceptualization, Formal Analysis, Resources, Writing - Original Draft, Visualization, Supervision, Project Administration, Funding Acquisition.

Data statement

The raw data are available online via the St. Lawrence Global Observatory (SLGO) database at https://doi.org/10.26071/ogsl-d3d5f1fa-a4d7.

Declaration of competing interest

The authors declare that they have no known competing financial interests or personal relationships that could have appeared to influence the work reported in this paper.

Acknowledgements

The authors thank the captain and crew of the Research Vessel *Nuliajuk* and Canadian Coast Guard Ship *Amundsen* as well as field personnel including M. Kendall and J. Kennedy, Government of Nunavut Fisheries and Sealing Division; S. Basso, Canada-Nunavut Geoscience Office; R. Deering and E. Edinger, Memorial University of Newfoundland; A. Buckley, University of Manitoba; and K. Polcwiartek, Centre for Earth Observation Science, University of Manitoba. We would like to thank C. Lewis (Fisheries and Oceans Canada), the Amaruq Hunters and Trappers Assocation, and the Nunavut Contaminants Committee for their input during the planning stages of the research. The Environmental Radiochemistry Laboratory supervised by D. Lobb assisted with radioisotope analysis. G. Stern provided laboratory access for PAH and mercury analysis, C. Spencer, Environment and Climate Change Canada, assisted with PFAS analysis. We thank L. Chow, K. Wiens, and E. Stainton from the Centre for Earth Observation Science for their assistance with logistics and administration. We acknowledge support from Canada's Excellence Research Chair program. P. Kimber assisted with graphic design. Sampling was funded by core activities within the Canada-Nunavut Geoscience Office, by the Canadian Northern Economic Development Agency's Strategic Investments in Northern Economic Development program and lab analysis was funded by Fisheries and Oceans Canada's Coastal Environmental Baseline Program. Additional funding was provided by the Natural Sciences and Engineering Research Council of Canada (NSERC) Discovery Grants program (Kuzyk), NCE ArcticNet (Kuzyk) and the University of Manitoba Graduate Fellowship (Bartley). Dr. Robie. W. Macdonald was an amazing scientist, researcher, mentor, and friend. The authors are honoured to submit our work to this special issue in his memory.

Appendix A. Supplementary data

Supplementary data to this article can be found online at https://doi.org/10.1016/j.ese.2023.100313.

References

[1] AMAP, "Human Health in the Arctic 2021. Summary for Policy-makers." p 16 (2021).
[2] Y. Yu, et al., Polycyclic aromatic hydrocarbons not declining in arctic air despite global emission reduction, Environ. Sci. Technol. 53 (5) (2019) 2375–2382, https://doi.org/10.1021/acs.est.8b05353.
[3] M.R. McCrystall, J. Stroeve, M. Serreze, B.C. Forbes, J.A. Screen, New climate models reveal faster and larger increases in Arctic precipitation than previously projected, Nat. Commun. 12 (1) (2021) 1–12, https://doi.org/10.1038/s41467-021-27031-y.
[4] R.W. Macdonald, Z.A. Kuzyk, S.C. Johannessen, It is not just about the ice: a geochemical perspective on the changing Arctic Ocean, J. Environ. Stud. Sci. 5 (3) (2015) 288–301, https://doi.org/10.1007/s13412-015-0302-4.
[5] W. Meier, J. Stroeve, An updated assessment of the changing arctic sea ice cover, Oceanography (2022), https://doi.org/10.5670/oceanog.2022.114.
[6] R.W. Macdonald, et al., Contaminants in the Canadian Arctic: 5 years of progress in understanding sources, occurrence and pathways, Sci. Total Environ. 254 (2000) 2–3.
[7] AMAP, Influence of climate change on transport, levels, and effects of contaminants in northern areas - Part 2, AMAP Tech. Rep. 10 (10) (2016) 1–52.
[8] L. Johnston, K. Reimer, S. Solomon, S. Harbicht, D. Bright, S. Parker, Baffin Region Ocean Disposal Investigation: Seabed Debris and Contaminant Inputs Near IqaluitResolution Island, Cape Dyer and Kivitoo, Department of National Defence, 1995.
[9] Z.A. Kuzyk, J.P. Stow, N.M. Burgess, S.M. Solomon, K.J. Reimer, PCBs in sediments and the coastal food web near a local contaminant source in Saglek Bay, Labrador, Sci. Total Environ. 351 (352) (2005) 264–284, https://doi.org/10.1016/j.scitotenv.2005.04.050.
[10] Z.Z.A. Kuzyk, N.M. Burgess, J.P. Stow, G.A. Fox, Biological effects of marine PCB contamination on black guillemot nestlings at Saglek, Labrador: liver biomarkers, Ecotoxicology 12 (1–4) (2003) 183–197, https://doi.org/10.1023/A:1022550709962.
[11] K.M. Stroski, K.H. Luong, J.K. Challis, L.G. Chaves-Barquero, M.L. Hanson, C.S. Wong, Wastewater sources of per- and polyfluorinated alkyl substances (PFAS) and pharmaceuticals in four Canadian Arctic communities, Sci. Total Environ. 708 (2020) 134494, https://doi.org/10.1016/j.scitotenv.2019.134494.
[12] J.E. Balmer, H. Hung, Y. Yu, R.J. Letcher, D.C.G. Muir, Sources and environmental fate of pyrogenic polycyclic aromatic hydrocarbons (PAHs) in the Arctic, Emerging Contam. 5 (2019) 128–142, https://doi.org/10.1016/j.emcon.2019.04.002.
[13] J.L. Kirk, et al., Mercury in Arctic marine ecosystems: sources, pathways and exposure, Environ. Res. 119 (2012) 64–87, https://doi.org/10.1016/j.envres.2012.08.012.
[14] J.J. MacInnis, I. Lehnherr, D.C.G. Muir, R. Quinlan, A.O. De Silva, Characterization of perfluoroalkyl substances in sediment cores from High and Low Arctic lakes in Canada, Sci. Total Environ. 666 (2019) 414–422, https://doi.org/10.1016/j.scitotenv.2019.02.210.
[15] D. Muir, et al., Levels and trends of poly- and perfluoroalkyl substances in the Arctic environment – an update, Emerging Contam. 5 (2019) 240–271, https://doi.org/10.1016/j.emcon.2019.06.002.
[16] H.M. Pickard, et al., Continuous non-marine inputs of per- and polyfluoroalkyl substances to the High Arctic: a multi-decadal temporal record, Atmos. Chem. Phys. 18 (7) (2018) 5045–5058, https://doi.org/10.5194/acp-18-5045-2018.
[17] K. Wang, K.M. Munson, A. Beaupré-Laperrière, A. Mucci, R.W. Macdonald, F. Wang, Subsurface seawater methylmercury maximum explains biotic mercury concentrations in the Canadian Arctic, Sci. Rep. 8 (1) (2018) 1–5, https://doi.org/10.1038/s41598-018-32760-0.
[18] L. Zhang, et al., Presence, sources and transport of polycyclic aromatic hydrocarbons in the Arctic Ocean, Geophys. Res. Lett. (2022), https://doi.org/10.1029/2022GL101496.
[19] K. Borgå, et al., The influence of global climate change on accumulation and toxicity of persistent organic pollutants and chemicals of emerging concern in Arctic food webs, Environ. Sci. Process. Impacts (2022), https://doi.org/10.1039/d1em00469g.

[20] K.A. Krumhansl, et al., Assessment of arctic community wastewater impacts on marine benthic invertebrates, Environ. Sci. Technol. 49 (2) (2015) 760–766, https://doi.org/10.1021/es503330n.
[21] G.M. Samuelson, Water and waste management issues in the Canadian Arctic: Iqaluit, Baffin Island, Can. Water Resour. J. 23 (4) (1998) 327–338, https://doi.org/10.4296/cwrj2304327.
[22] T. Tremblay, C.M. Kamula, S. Ciastek, Z.A. Kuzyk, Overview of the Geochemical Properties of the Marine Sediments of Koojesse Inlet, Frobisher Bay, Nunavut, Canada-Nunavut Geosci. Off., 2020, pp. 125–144.
[23] Statistics Canada, Census profile, 2016 census, Iqaluit, Nunavut and Nunavut, Statistics Canada. https://www12.statcan.gc.ca/census-recensement/2016/dp-pd/prof/details/page.cfm?Lang=E&Geo1=CSD&Code1=6204003&Geo2=PR&Code2=62&SearchText=Iqaluit&SearchType=Begins&SearchPR=01&B1=All&GeoLevel=PR&GeoCode=6204003&TABID=1&type=0.
[24] G.M. Samuelson, Polychaetes as indicators of environmental disturbance on subarctic tidal flats, Iqaluit, Baffin Island, Nunavut Territory, Mar. Pollut. Bull. 42 (9) (2001) 733–741, https://doi.org/10.1016/S0025-326X(00)00208-3.
[25] S. Weichenthal, et al., The impact of a landfill fire on ambient air quality in the north: a case study in Iqaluit, Canada, Environ. Res. 142 (2015) 46–50, https://doi.org/10.1016/j.envres.2015.06.018.
[26] R.V. Eno, Crystal two: the origin of Iqaluit, Arctic 56 (1) (2003) 63–75.
[27] J.S. Poland, S. Mitchell, A. Rutter, Remediation of former military bases in the Canadian Arctic, Cold Reg. Sci. Technol. 32 (2–3) (2001) 93–105, https://doi.org/10.1016/S0165-232X(00)00022-7.
[28] AMAP, AMAP Assessment 2021: Mercury in the Arctic, Tromsø, Norway, 2021.
[29] N. Carter, J. Dawson, J. Joyce, A. Ogilvie, "Arctic corridors and northern voices, in: Governing Marine Transportation in the Canadian Arctic: Arviat, Nunavut, vol. 44, Univ. Ottawa, 2018, https://doi.org/10.20381/RUOR38038.
[30] C.M. Schaefer, D. Deslauriers, K.M. Jeffries, "The truncate soft-shell clam, *Mya truncata*, as a biomonitor of municipal wastewater exposure and historical anthropogenic impacts in the Canadian Arctic", Can. J. Fish. Aquat. Sci. 79 (3) (2022) 367–379, https://doi.org/10.1139/cjfas-2021-0078.
[31] I.R. Hilgendag, H.K. Swanson, C.W. Lewis, A.D. Ehrman, M. Power, Mercury biomagnification in benthic, pelagic, and benthopelagic food webs in an Arctic marine ecosystem, Sci. Total Environ. (2022) 156424, https://doi.org/10.1016/j.scitotenv.2022.156424.
[32] A. Corminboeuf, J.C. Montero-Serrano, R. St-Louis, Spatial and temporal distributions of polycyclic aromatic hydrocarbons in sediments from the Canadian Arctic Archipelago, Mar. Pollut. Bull. 171 (January) (2021) 112729, https://doi.org/10.1016/j.marpolbul.2021.112729.
[33] B.J. Todd, J. Shaw, D.C. Campbell, D.J. Mate, Preliminary Interpretation of the Marine Geology of Frobisher Bay, Baffin Is-Land, Nunavut; in Summary of Activities, Canada-Nunavut Geosci. Off., 2016, pp. 61–66 [Online]. Available: http://cngo.ca/summary-of-activities/2016/.
[34] E.C. Herder, TEMPORAL AND SPATIAL CHANGES IN BENTHIC MOLLUSC (BIVALVES AND GASTROPODS) COMMUNITIES IN INNER FROBISHER BAY, NUNAVUT, BAFFIN ISLAND OVER FIFTY YEARS, Memorial University of Newfoundland, 2020.
[35] S.V. Hatcher, D.L. Forbes, Exposure to coastal hazards in a rapidly expanding northern urban centre, Iqaluit, Nunavut, Arctic 68 (4) (2015) 453–471, https://doi.org/10.14430/arctic4526.
[36] J.D. Eakins, R.T. Morrison, A new procedure for the determination of lead-210 in lake and marine sediments, Int. J. Appl. Radiat. Isot. 29 (9–10) (1978) 531–536, https://doi.org/10.1016/0020-708X(78)90161-8.
[37] Z.Z.A. Kuzyk, R.W. Macdonald, S.C. Johannessen, Calculating Rates and Dates and Interpreting Contaminant Profiles in Biomixed Sediments, in: J. Blais, M. Rosen, J. Smol (Eds.), Environmental Contaminants. Developments in Paleoenvironmental Research, 18, Springer, Dordrecht, 2015, pp. 61–87.. https://doi.org/10.1007/978-94-017-9541-8_4.
[38] R. R Core Team, A Language and Environment for Statistical Computing, R Foundation for Statistical Computing, Vienna, Austria, 2023. https://www.r-project.org/.
[39] J. Mastin, T. Harner, J.K. Schuster, L. South, A review of PCB-11 and other unintentionally produced PCB congeners in outdoor air, Atmos. Pollut. Res. 13 (4) (2022) 101364, https://doi.org/10.1016/j.apr.2022.101364.
[40] ASTDR, Toxicological Profile for Polychlorinated Biphenyls (PCBs), 2000. Atlanta, GA.
[41] Z.Z.A. Kuzyk, C. Gobeil, R.W. Macdonald, 137Cs in margin sediments of the Arctic Ocean: controls on boundary scavenging.", Global Biogeochem. Cycles 27 (2) (2013) 422–439, https://doi.org/10.1002/gbc.20041.
[42] R. Deering, et al., "Characterization of the seabed and postglacial sediments of inner frobisher bay, baffin island, Nunavut," Canada-Nunavut Geosci. Off (2018) 139–152 [Online]. Available: http://cngo.ca/summary-of-activities/2018/.
[43] M.A. Monetti, Worldwide Deposition of Strontium-90 through 1990, USDOE Environmental Measurements Lab, New York, 1996, p. 60.
[44] Z.Z.A. Kuzyk, R.W. Macdonald, S.C. Johannessen, C. Gobeil, G.A. Stern, Towards a sediment and organic carbon budget for Hudson Bay, Mar. Geol. 264 (3–4) (2009) 190–208, https://doi.org/10.1016/j.margeo.2009.05.006.
[45] M.A. Goñi, A.E. O'Connor, Z.Z. Kuzyk, M.B. Yunker, C. Gobeil, R.W. Macdonald, Distribution and sources of organic matter in surface marine sediments across the North American Arctic margin, J. Geophys. Res. Ocean. 118 (9) (2013) 4017–4035, https://doi.org/10.1002/jgrc.20286.
[46] C.J. Schubert, S.E. Calvert, Nitrogen and carbon isotopic composition of marine and terrestrial organic matter in Arctic Ocean sediments: implications for nutrient utilization and organic matter composition, Deep. Res. I 48 (2001) 789–810.
[47] R. Stein, R.W. Macdonald, The Organic Carbon Cycle in the Arctic Ocean, Springer Publishing Company, Berlin, 2004.
[48] C.M. Kamula, Z.Z.A. Kuzyk, D.A. Lobb, R.W. Macdonald, Sources and accumulation of sediment and particulate organic carbon in a subarctic fjard estuary: 210Pb,137Cs, and δ13C records from lake melville, labrador, Can. J. Earth Sci. 54 (9) (2017) 993–1006, https://doi.org/10.1139/cjes-2016-0167.
[49] M.B. Yunker, R.W. Macdonald, R. Vingarzan, R.H. Mitchell, D. Goyette, S. Sylvestre, PAHs in the Fraser River basin: a critical appraisal of PAH ratios as indicators of PAH source and composition, Org. Geochem. 33 (4) (2002) 489–515, https://doi.org/10.1016/S0146-6380(02)00002-5.
[50] Z.Z.A. Kuzyk, R.W. MacDonald, S.C. Johannessen, G.A. Stern, Biogeochemical controls on PCB deposition in Hudson bay, Environ. Sci. Technol. 44 (9) (2010) 3280–3285, https://doi.org/10.1021/es903832t.
[51] The MathWorks Inc., MATLAB Version: 9.13.0 (R2022b), The MathWorks Inc., Natick, Massachusetts, 2022. https://www.mathworks.com.
[52] H. Joerss, C. Apel, R. Ebinghaus, Emerging per- and polyfluoroalkyl substances (PFASs) in surface water and sediment of the North and Baltic Seas, Sci. Total Environ. 686 (2019) 360–369, https://doi.org/10.1016/j.scitotenv.2019.05.363.
[53] Y. Lin, et al., Perfluoroalkyl substances in sediments from the Bering Sea to the western Arctic: source and pathway analysis, Environ. Int. 139 (April) (2020) 105699, https://doi.org/10.1016/j.envint.2020.105699.
[54] C.A. Moody, J.A. Field, Perfluorinated surfactants and the environmental implications of their use in fire-fighting foams, Environ. Sci. Technol. 34 (18) (2000) 3864–3870, https://doi.org/10.1021/es991359u.
[55] M.M. Phillips, M.J.A. Dinglasan-Panlilio, S.A. Mabury, K.R. Solomon, P.K. Sibley, Fluorotelomer acids are more toxic than perfluorinated acids, Environ. Sci. Technol. 41 (20) (2007) 7159–7163, https://doi.org/10.1021/es070734c.
[56] D.A. Ellis, et al., Degradation of fluorotelomer alcohols: a likely atmospheric source of perfluorinated carboxylic acids, Environ. Sci. Technol. 38 (12) (2004) 3316–3321, https://doi.org/10.1021/es049860w.
[57] J. Carrie, F. Wang, H. Sanei, R.W. Macdonald, P.M. Outridge, G.A. Stern, Increasing contaminant burdens in an arctic fish, burbot (Lota lota), in a warming climate, Environ. Sci. Technol. 44 (1) (2010) 316–322, https://doi.org/10.1021/es902582y.
[58] A.A. Hare, G.A. Stern, Z.Z.A. Kuzyk, R.W. MacDonald, S.C. Johannessen, F. Wang, Natural and anthropogenic mercury distribution in marine sediments from Hudson Bay, Canada, Environ. Sci. Technol. 44 (15) (2010) 5805–5811, https://doi.org/10.1021/es100724y.
[59] D.A. Bright, W.T. Dushenko, S.L. Grundy, K.J. Reimer, Effects of local and distant contaminant sources: polychlorinated biphenyls and other organochlorines in bottom-dwelling animals from an Arctic estuary, Sci. Total Environ. 160–161 (1995) 265–283, https://doi.org/10.1016/0048-9697(95)04362-5. C.
[60] D.A. Bright, W.T. Dushenko, S.L. Grundy, K.J. Reimer, Evidence for short-range transport of polychlorinated biphenyls in the Canadian Arctic using congener signatures of PCBs in soils, Sci. Total Environ. 160–161 (1995) 251–263, https://doi.org/10.1016/0048-9697(95)04361-4. C.
[61] D.G. Streets, H.M. Horowitz, Z. Lu, L. Levin, C.P. Thackray, E.M. Sunderland, Global and regional trends in mercury emissions and concentrations, 2010–2015, Atmos. Environ. 201 (2019) 417–427, https://doi.org/10.1016/j.atmosenv.2018.12.031. December 2018.
[62] D.G. Streets, et al., Total mercury released to the environment by human activities, Environ. Sci. Technol. 51 (11) (2017) 5969–5977, https://doi.org/10.1021/acs.est.7b00451.
[63] H. Shen, et al., Global atmospheric emissions of polycyclic aromatic hydrocarbons from 1960 to 2008 and future predictions, Environ. Sci. Technol. 47 (2013) 6415–6424.
[64] K. Breivik, A. Sweetman, J.M. Pacyna, K.C. Jones, Towards a global historical emission inventory for selected PCB congeners - a mass balance approach: 2. Emissions, Sci. Total Environ. 290 (1–3) (2002) 199–224, https://doi.org/10.1016/S0048-9697(01)01076-2.
[65] Z. Wang, I.T. Cousins, M. Scheringer, R.C. Buck, K. Hungerbühler, Global emission inventories for C4-C14 perfluoroalkyl carboxylic acid (PFCA) homologues from 1951 to 2030, Part I: production and emissions from quantifiable sources, Environ. Int. 70 (2014) 62–75, https://doi.org/10.1016/j.envint.2014.04.013.
[66] D.A. Bright, S.L. Grundy, K.J. Reimer, Differential bioaccumulation of non-ortho-substituted and other PCB congeners in coastal arctic invertebrates and fish, Environ. Sci. Technol. 29 (10) (1995) 2504–2512, https://doi.org/10.1021/es00010a008.